

HYDROCRACKING OF COAL AND PETROLEUM OILS

S. A. Qader and G. R. Hill

Department of Mineral Engineering

University of Utah, Salt Lake City, Utah 84112.

Abstract

Hydrocracking of coal-based oils needs higher hydrogen pressure when compared to petroleum oils and both types of oils affect almost similar naphtha yields of 77 to 80% at a pressure of 2000 p.s.i. and 500°C. Coal-based oils produce naphtha of superior quality but with higher hydrogen consumption. At about 80% yield, naphtha from coal oil had a clear research octane number of 88 with a hydrogen consumption of about 1550 cu. ft. per barrel of feed, whereas the product from gas oil has an octane number of 78 with a hydrogen consumption of only about 1125 cu. ft. Both types of oils exhibited similar kinetic behavior with activation energies ranging from 14,000 to 16,000 cal./mole. The hydrocracking of coal-based and petroleum oils must be preceded by the hydrorefining of the feed stocks to ensure low coke yield and longer catalyst life. The disadvantages associated with the processing of coal-based oils can be offset by the superior quality of their products, thereby affecting the overall processing almost similar to petroleum oils.

Introduction

Hydrocracking is employed in the petroleum industry, in recent years, for the processing of different types of feed stocks (Craig and Forster, 1966; Duir, 1967). It was also applied as a potential method for the refining of coal-derived liquids (Alpert, et al., 1966, Katsobashvili and Elbert,

1966). The hydrocracking of coal-based oils differs to some extent from petroleum oils since the former contain larger quantities of oxygenated compounds and aromatic hydrocarbons. In view of the anticipated shortage of crude petroleum, the petroleum refineries may have to augment their feed stocks with synthetic oils and process them in the existing equipment. The additional oil requirements may be met in the near future from coal liquifaction processes and, hence, it is necessary and useful to understand the fundamental differences that may exist between the refining of petroleum and coal-based oils. Hydrocracking is a versatile processing method and it may be valuable to study and compare the behavior of petroleum and coal-based oils under hydrocracking conditions. The fundamental aspects of hydrocracking of petroleum and coal-based oils are not well understood at the present time though some work was earlier reported mainly on the study of product distributions or catalyst performance (Carpenter, et al., 1963; Archibald, et al., 1960). Some data, however, were reported on the mechanism of hydrocracking of some pure hydrocarbons (Archibald, et al., 1960; Flinn, et al., 1960). In the present communication, the results of hydrocracking of three petroleum fractions and two coal-based oil fractions are reported. A comparison was made between the petroleum and coal-based oils with respect to their behavior under hydrocracking conditions.

Experimental

Materials.

The petroleum fractions were obtained from a mixed base crude oil by atmospheric distillation. The coal oil was obtained from a high volatile bituminous coal by hydrogenation in an entrained bed reactor unit at 2000 p.s.i. pressure and 510°C with stannous chloride as the catalyst. Low

temperature tar was prepared from the same coal in a laboratory oven at 580°C. The coal oil and tar fractions were obtained by distillation of the whole oils, respectively. The hydrorefining catalyst contained 3% cobalt oxide and 12% molybdenum trioxide supported on alumina in the form of pellets of 0.083-inch diameter and 0.125-inch height with a surface area of 210 sq. meters per gram. The hydrocracking catalyst contained 6% nickel sulfide and 19% tungsten disulfide supported on silica-alumina in the form of pellets of 0.083-inch diameter and 0.125-inch height with a surface area of 198 sq. meters per gram.

Equipment.

The hydrocracking unit (Figure 1) contained a vertical tubular stainless steel reactor of 0.75-inch inside diameter and 40-inch length with precision equipment for controlling temperature, pressure, and gas and liquid flow rates. The reactor was heated uniformly by a tubular ceramic furnace of 1.5-inch inside diameter and 38-inch length. The first 20-inch length of the reactor from the top was packed with ceramic beads of 0.17-inch diameter, the next 6.5 inches with the catalyst (60 c-c), and the following 12 inches again with ceramic beads. The temperature of the catalyst bed was maintained constant and the reaction temperature was measured by a thermocouple placed at the center of the catalyst bed. The hydrogen supply was taken from hydrogen tanks. The hydrorefining was also done in the same unit but with the refining catalyst.

Hydrocracking procedure.

The whole system was first flushed with hydrogen to remove air, pressurized, and heated to the reactor temperature. The pressure was then adjusted to the experimental pressure and the oil was fed at the desired rate. The

initial one hour was taken as an offstream period for bringing the reactor and the product recovery system to equilibrium. The hydrogen to oil feed ratio was maintained at about 500. The values of space velocities varied in the range of $\pm 10\%$ and were rounded off. The product was cooled in the condenser and the liquid product was collected in the separator. The gaseous product containing some uncondensed oil was passed through an active carbon tower to adsorb the oil and a gas meter to measure the rate and total volume passed. Several gas samples were withdrawn during each experiment for analysis. The difference in the weight of active carbon before and after the experiment was taken as the amount of uncondensed naphtha. The yield of the liquid product varied between 95 and 100% with an initial boiling point between 50° and 65°C . The yield of gas and each hydrocarbon component of the gas were calculated from the total gas and its composition. The liquid product was distilled and the fraction boiling up to 200°C was designated as naphtha. The fraction boiling up to 100°C was designated as light naphtha and the fraction boiling from 100° to 200°C as heavy naphtha. The hydrorefining was also done in a similar manner at 1500 p.s.i. pressure, 425°C , and 1-space velocity. All the products reported are double-pass products and the product distribution data were obtained at a space velocity of about 0.5. Cumene was hydrocracked over the fresh catalyst and also intermittently during the experimental work to test the activity of the catalyst. The catalyst was either regenerated or replaced by fresh catalyst when the activity with respect to cumene cracking fell by about 5 percentage points.

Coke determination.

The used catalyst was taken out from the reactor and dried at 110°C for two hours to remove moisture and volatile hydrocarbons. Twenty-five grams of

the dried catalyst was packed in a glass tube of 0.5-inch internal diameter and 12-inch length heated to 600°C by a tubular furnace. A stream of air was passed through the tube at the rate of about 15 c.c per minute and the effluent was passed through a furnace containing cupric oxide at 700°C to oxidize carbon monoxide to carbon dioxide, a tower containing Drierite to adsorb any moisture and a tower of Ascarite to adsorb carbon dioxide. The carbon on the catalyst was calculated from the weight of carbon dioxide and reported as coke. The catalyst deposit was not strictly carbon but coke containing both carbon and hydrogen. The coke values reported actually refer to the carbon content of the coke, the latter amounting to about 95% of the former, the remaining being hydrogen.

Product analysis.

All the analyses of the liquid products were done by ASTM and other standard methods and gaseous products by gas chromatographic and mass spectrometric methods (Qader and Hill, 1969).

Results and Discussion

The yield of naphtha from petroleum fractions increased linearly with the reaction temperature. The stove, diesel, and gas oils yielded a maximum of 79, 78, and 77% naphtha at 1500 p.s.i. pressure and 79, 80, and 79% at 2000 p.s.i. pressure and 500°C, respectively. Increasing the reaction pressure from 1500 to 2000 p.s.i. did not change the naphtha yield to any appreciable extent (Figure 2). On the other hand, the naphtha yield from coal-based oils was increased significantly with an increase in the hydrogen pressure. The coal oil and low temperature tar yielded a maximum of 63 and 60% naphtha at 1500 p.s.i. pressure and 79 and 77% at 2000 p.s.i. pressure and 500°C, respectively. The yield of naphtha did not vary linearly with temperature at 1500 p.s.i. pressure while it was linear at a pressure of 2000 p.s.i. The effect was more pronounced at temperatures above 450°C (Figure 3). The results

indicate that the hydrocracking of coal-based oils needs higher hydrogen pressures when compared to the petroleum oils and both types of oils affect almost similar naphtha yields at a pressure of 2000 p.s.i. In case of coal oils, the higher hydrogen pressure is needed for the hydrogenation of aromatic hydrocarbons and the heterocyclic compounds. At pressures of 2000 p.s.i. and above, the petroleum and coal oils exhibit similar behavior under hydrocracking conditions.

The API gravity and the characterization factor of a liquid fuel mainly depend upon its boiling range and the aromatic hydrocarbon content. In case of petroleum oils investigated, the characterization factor increased with a decrease in gravity (Figure 4) which appears to be mainly due to the differences in the boiling ranges of the feed stocks since they have similar composition (Table 1). Though a similar relationship was exhibited by coal-based oils (Figure 4), the factors contributing to such a behavior seem to be different. While the lower gravity of the coal oil when compared to coal tar may be due to the differences in the boiling ranges and aromatic contents of the oils, the high characterization factor of the coal oil does not seem to commensurate with a slight difference in the boiling range and the aromatic hydrocarbons. The characterization factor might have been influenced by the presence of higher concentrations of hydroaromatics in the coal oil. This is further evidenced by the higher naphtha yield from coal oil at 1500 p.s.i. pressure (Figures 5 and 6) where the hydrogenation of aromatics to the corresponding hydroaromatics which undergo subsequent cracking does not occur to any appreciable extent (Qader, et al., 1968). However, hydrogenation of aromatics to the corresponding hydroaromatics does take place at a pressure of 2000 p.s.i., thereby narrowing down the gap between naphtha yields from coal oil

and coal tar fractions as shown in Figures 5 and 6. The increase in the yield of naphtha with gravity and the decrease with characterization factor of petroleum fractions (Figures 5 and 6) are mainly due to the differences in their boiling ranges.

The product distribution data indicated that the hydrocracking of petroleum fractions produces higher quantities of gaseous product when compared to coal-based oils at all levels of naphtha formation (Figure 7). Coal-based oils produced more C₁-C₃ hydrocarbons than petroleum oils at different levels of butane production (Figure 8). The production of +200°C oil fraction was higher in the hydrocracking of coal-based oils. However, the differences are not large enough to alter the product distribution significantly. Isomerization is an important aspect of hydrocracking and the results shown in Figure 9 indicated the occurrence of more isomerization in the hydrocracking of petroleum oils when compared to the coal-based oils at all levels of naphtha formation. The iso-normal ratios in butanes varied between 1 and 4 in the case of petroleum oils, while the ratios varied between 1 and 2.75 in the case of coal-based oils. Occurrence of isomerization during hydrocracking produces better quality naphtha and this is an advantage associated with the petroleum oils under hydrocracking conditions. However, there may be several other factors which influence the quality of naphtha. The relative proportions of light and heavy fractions of naphtha will also contribute to the overall quality of the naphtha. Normally light naphthas produced from petroleum fractions have higher octane ratings than heavy naphthas, necessitating the subsequent reforming of heavy naphtha. The results in Figures 10 and 11 indicated that petroleum oils produce more light naphtha relative to heavy naphtha when compared to coal-based oils. The ratios of heavy-light naphthas varied

between 2 and 4 in the case of petroleum oils, while the ratios varied between 3.5 and 4.5 in the case of coal-based oils. This is again an added advantage associated with petroleum oils, though this is not the final deciding factor.

The hydrocarbon composition of naphthas obtained from petroleum and coal-based oils was shown in Figure 12. Coal-based naphthas contained higher proportions of aromatic hydrocarbons than petroleum naphthas. At about 80% formation, petroleum naphthas contained about 35 to 40%, while coal-based naphthas contained about 55% aromatic hydrocarbons. This may make a great difference in the octane rating of the naphthas and coal-based naphthas are expected to have high octane values. Petroleum naphthas contained slightly higher concentrations of naphthenes and isoparaffins than coal-based naphthas, while the contents of normal paraffins and olefins were almost the same in both cases. The quality of coal-based naphthas was found to be much superior to the petroleum naphthas, as shown in Figure 13. The clear research octane numbers of coal-based naphthas varied between about 80 to 90, while the octane numbers of the petroleum naphthas varied only in between about 65 to 80. At the maximum yield of about 80%, coal-based naphthas had clear research octane numbers of about 90, while the octane ratings were below 80 numbers in the case of petroleum naphthas. The coal-based naphthas can be used as regular grade gasoline without further treatment and as premium grade product simply by the use of additives. Petroleum naphthas need to be reformed before they can be used either as regular or premium grade materials. Coal-based naphthas have slightly higher concentrations of sulfur and nitrogen which, however, are much below the specified limits.

Hydrogen requirement is an important factor which contributes significantly to the overall refining cost of fuel oils. The results shown in Figure 14

illustrated that hydrogen consumption was high in the hydrocracking of coal-based oils when compared to petroleum oils. At the maximum yield of about 80% naphtha, hydrogen consumption varied between 800 to 1100 and 1500 to 1600 cu. ft. per barrel of feed stock in the hydrocracking of petroleum and coal-based oils, respectively. The high hydrogen consumption in the case of coal-based oils was due to the hydrogenation of aromatic hydrocarbons and heterocyclic compounds, especially the oxygenated compounds. This is one of the disadvantages associated with the refining of coal-based oils.

Kinetics

For the kinetic study the gas oil and coal oil fractions were used and the hydrocracking experiments were conducted at a constant hydrogen pressure of 2000 p.s.i. The overall rates of hydrocracking were studied by the application of Equation 1 assuming first-order kinetics (Qader and Hill, 1969).

$$\ln \frac{X_i}{X_f} = k \frac{1}{\text{LHSV}} \quad (1)$$

where

X_i = initial concentration of the reactant, wt. %

X_f = final concentration of the reactant, wt. %

LHSV = liquid hourly space velocity, volume of liquid feed per hour per volume of catalyst

k = specific reaction rate constant

The plots of reciprocal space velocity versus $\log \frac{X_i}{X_f}$ are shown in Figures 15 and 16. The plots were linear and, thus, the first-order rate constants can be represented by Equations 2 and 3.

$$-\frac{d(\text{gas oil})}{dt} = k_g (\text{gas oil}) \quad (2)$$

$$-\frac{d(\text{coal oil})}{dt} = k_c (\text{coal oil}) \quad (3)$$

where k_g and k_c are rate constants for gas oil and coal oil hydrocracking, respectively. The Arrhenius plots (Figure 17) were linear and the rate constants were found to be represented by Equations 4 and 5.

$$k_g = 0.3651 \times 10^4 e^{-14,300/RT} \text{ hr.}^{-1} \quad (4)$$

$$k_c = 0.8395 \times 10^4 e^{-15,500/RT} \text{ hr.}^{-1} \quad (5)$$

The following values of enthalpies and entropies of activation were calculated from plots of $\log \frac{k}{T}$ versus $\frac{1}{T}$ by applying Eyring equation (Figure 18).

$$\Delta H_g^\ddagger = 12,800 \text{ cal./mole}, \quad \Delta S_g^\ddagger = -52 \text{ e.u.}$$

$$\Delta H_c^\ddagger = 1,400 \text{ cal./mole}, \quad \Delta S_c^\ddagger = -50 \text{ e.u.}$$

The kinetic data indicates that both the gas oil and coal oil exhibit similar kinetic behavior under hydrocracking conditions except the coal oil needs a slightly higher activation energy. The mechanisms of hydrocracking of gas oil and the coal oil appear to be similar as proposed earlier and the energetics suggest that chemical reactions involving the cracking of C-C, C-O, C-S, and C-N bonds will control the reaction rate (Qader, et al., 1968 and 1969). The catalyst used in this investigation is a dual-functional one, containing both a cracking component and a hydrogenation component. Since cracking is the rate controlling step in hydrocracking, the reaction rates and the product yields are mainly influenced by the activity of the cracking component of the catalyst. Therefore, it is essential to carry out the hydrocracking process under conditions wherein the cracking component maintains high activity. The cracking activity of the catalyst is due to the acidic surface sites of silica which may get poisoned due to the accumulation of coke and the basic nitrogen compounds. The coke formation may also reduce the activity of the hydrogenation component of the catalyst. Therefore, it is important to study the coke deposition on the catalyst during hydrocracking. Figure 19 shows the coke

deposition on the catalyst by the hydrocracking of gas oil and coal oil at a temperature of 480°C, 2000 p.s.i. pressure, and 1-space velocity. The coke formation by the coal oil was almost double the amount by the gas oil, which suggests that the catalyst life will be shortened to a great degree during the hydrocracking of coal oil. This may make the hydrocracking of coal oil more expensive when compared to the gas oil. However, if the feed stocks are hydrorefined in a preceding step to remove the nitrogen compounds which otherwise will poison the acidic sites of the cracking component of the catalyst during hydrocracking, the coke formation on the catalyst can be reduced to a great extent as shown in Figure 20. Further, the gas oil and the coal oil affect almost the same amount of coke deposition on the catalyst during the hydrocracking of the hydrorefined feed stocks. The results suggest that the hydrocracking of either petroleum or coal-based oils on the dual-functional catalyst must be preceded by the hydrorefining of the feed stocks and the hydrocracking of the preredefined feed stocks will exhibit similar characteristics with respect to catalyst requirements. This investigation indicates that though the hydrocracking of petroleum oils has certain advantages over the coal-based oils, the disadvantages associated with the latter may be offset by the superior quality of their products, thereby affecting the overall processing of both types of oils almost similarly.

Table 1. Properties of feed materials.

	Stove oil	Diesel oil	Gas oil	Coal oil fraction	Low tem- perature tar fraction
Gravity, °API	38.2	36.5	32.4	21.5	23.4
Characterization factor	11.2	11.6	11.9	9.9	9.5
Sulfur, wt. %	0.24	0.22	0.38	0.62	0.84
Nitrogen, wt. %	0.18	0.16	0.14	0.42	0.58
Oxygen, wt. %	Nil	Nil	Nil	3.6	4.8
Distillation					
I.B.P., °C	200	250	350	200	200
50%	250	302	430	238	260
F.B.P., °C	300	380	490	370	360
Hydrocarbon analysis, vol. %					
Saturates	80	80	81	38	28
Aromatics	20	20	19	57	54
Olefins	Nil	Nil	Nil	5	18

Literature Cited

1. Alpert, S. P., Johanson, E. S., Schuman, S. C., Chem Eng. Progress, 60, No. 6, 35 (1964).
2. Archibald, R. C., Greensfelder, B. S., Holzman, G., Rowf, D. H., Ind. Eng. Chem., 52, 745 (1960).
3. Carpenter, H. C., Cottingham, P. L., Frost, C. M., Fowkes, W. W., Bureau of Mines Report of Investigation, No. 6237 (1963).
4. Craig, R. G., Forster, H. A., Oil Gas J., 45, 159 (1966).
5. Duir, J. H., Hydrocarbon Processing and Petrol. Refiner, 46, 127 (1967).
6. Flinn, R. A., Larson, O. A., Beuther, H., Ind. Eng. Chem., 52, 153 (1960).
7. Katsobashvili, Ya. R., Elbert, E. A., Coke and Chemistry, U.S.S.R., 1, 41 (1966).
8. Qader, S. A., Wiser, W. H., Hill, G. R., Preprints, 155th National Meeting, ACS, Division of Fuel Chemistry, 12, No. 2, 28 (1968).
9. Qader, S. A., Wiser, W. H., Hill, G. R., Ind. Eng. Chem. Proc. Res. Develop., 7, 390 (1968).
10. Qader, S. A., Hill, G. R., Ind. Eng. Chem. Proc. Res. Develop., 1, (1969).
11. Zielke, C. W., Struck, R. T., Evans, J. M., Costanza, C. P., Gorn, E., Ind. Eng. Chem., 5, 151 and 158 (1966).

Acknowledgement

Research work supported by the Office of Coal Research and the University of Utah.

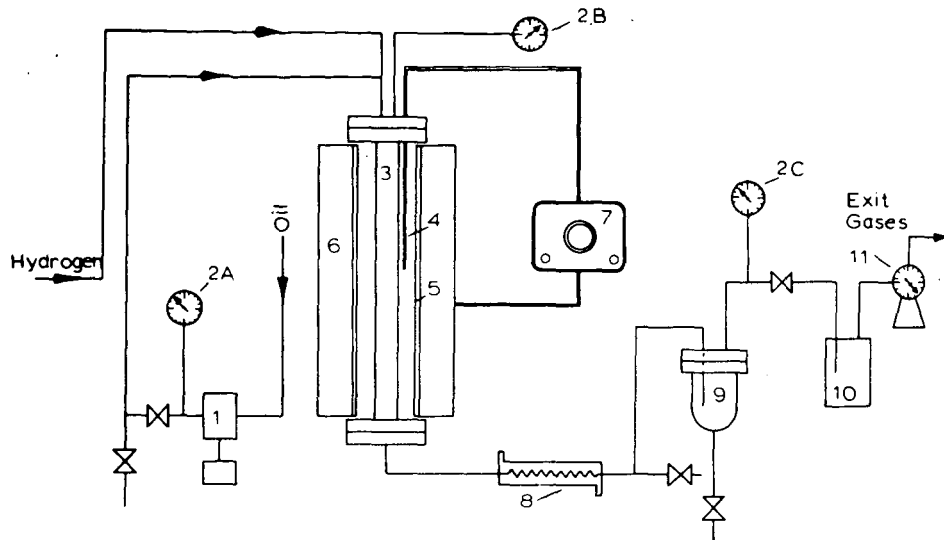


FIGURE 1. FLOW SHEET OF THE HYDROTREATING UNIT.
 1. HIGH PRESSURE PUMP, 2A, 2B, 2C. PRESSURE GAUGE, 3. REACTOR, 4. THERMOCOUPLE,
 5. CERAMIC FURNACE, 6. INSULATION, 7. TEMPERATURE CONTROLLER, 8. CONDENSER,
 9. SEPARATOR, 10. ACTIVE CARBON TOWER, 11. GAS METER.

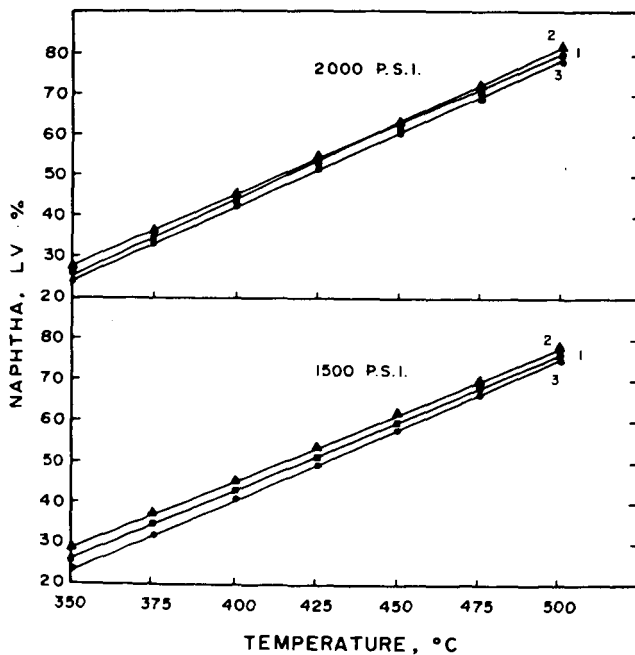


FIGURE 2. INFLUENCE OF TEMPERATURE AND PRESSURE ON NAPHTHA YIELD.
 1. STOVE OIL, 2. DIESEL OIL, 3. GAS OIL.

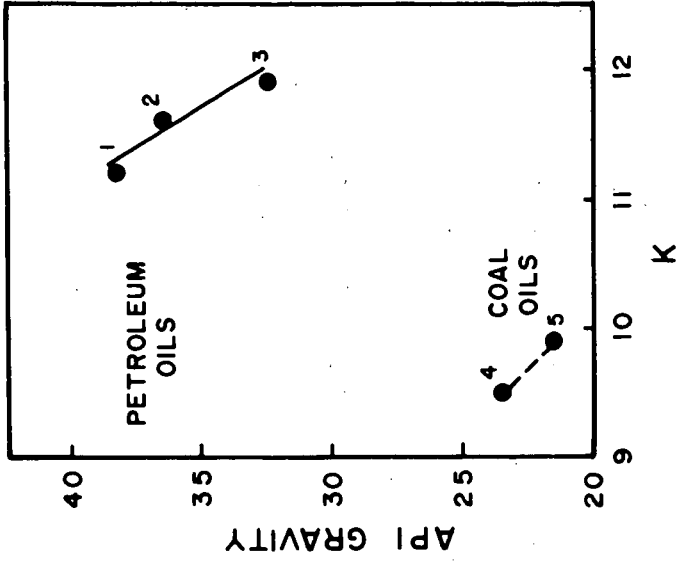


FIGURE 4. RELATIONSHIP BETWEEN GRAVITY AND CHARACTERIZATION FACTOR.
 1. STOVE OIL, 2. DIESEL OIL, 3. GAS OIL, 4. LOW TEMPERATURE TAR, 5. COAL OIL.

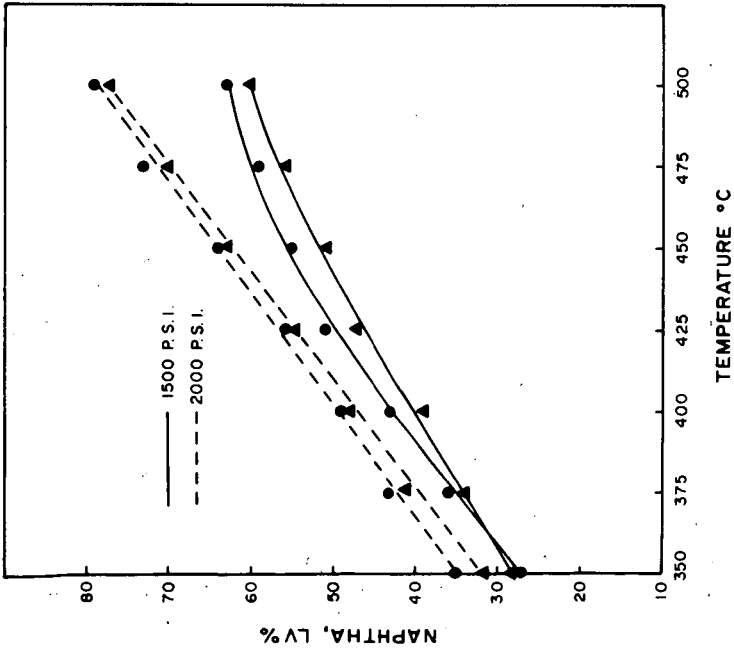


FIGURE 3. INFLUENCE OF TEMPERATURE AND PRESSURE ON NAPHTHA YIELD.
 1. COAL OIL, 2. LOW TEMPERATURE TAR.

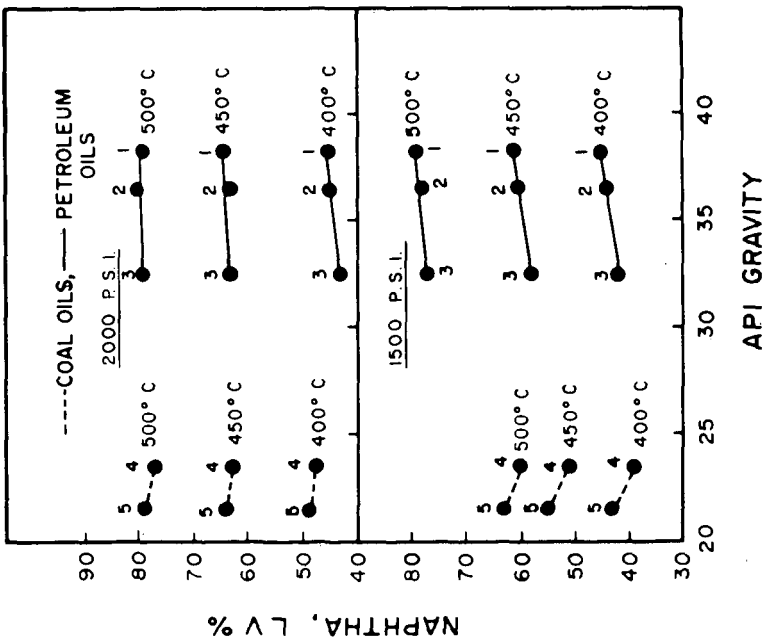


FIGURE 5. RELATIONSHIP BETWEEN NAPHTHA YIELD AND GRAVITY OF FEED STOCKS.
 1. STOVE OIL, 2. DIESEL OIL, 3. GAS OIL, 4. LOW TEMPERATURE TAR, 5. COAL OIL.

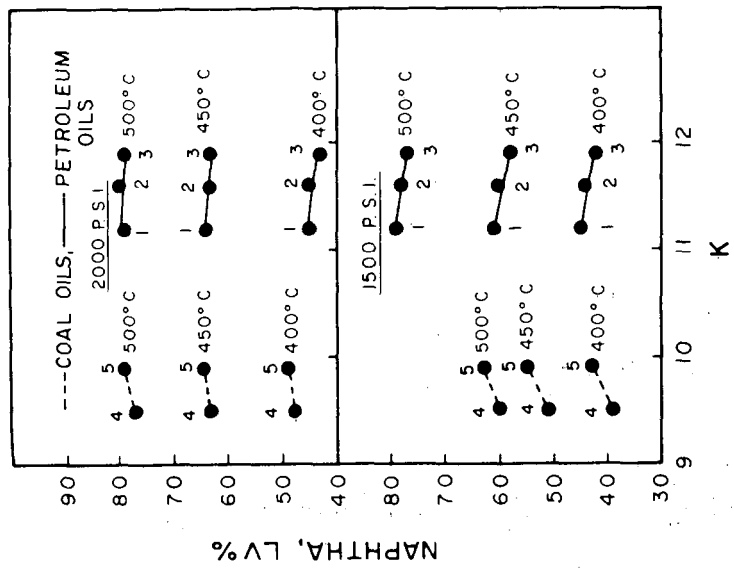


FIGURE 6. RELATIONSHIP BETWEEN NAPHTHA YIELD AND FEED TEMPERATURE FACTOR OF FEED STOCKS.
 1. STOVE OIL, 2. DIESEL OIL, 3. GAS OIL, 4. LOW TEMPERATURE TAR, 5. COAL OIL.

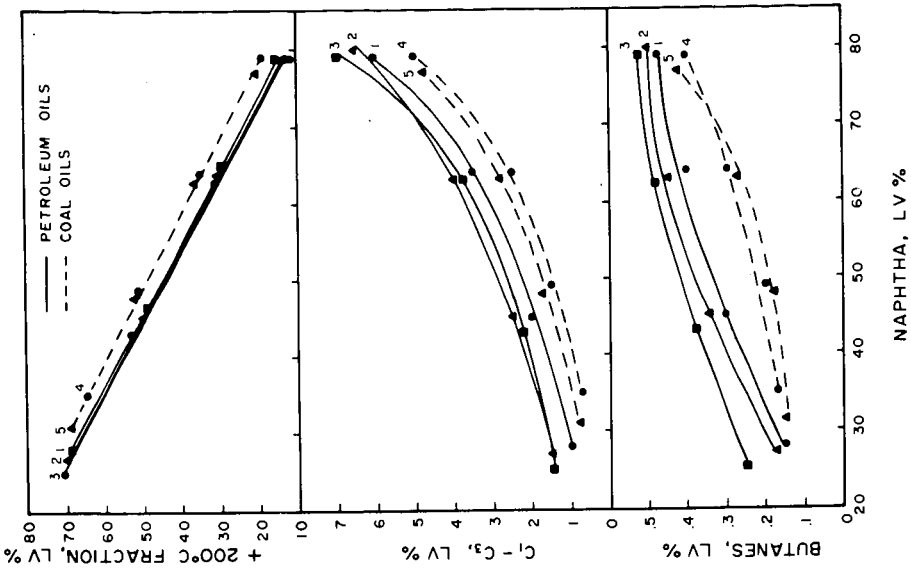


FIGURE 7. PRODUCT DISTRIBUTION AT DIFFERENT LEVELS OF NAPHTHAM YIELD.
 1. STOVE OIL, 2. DIESEL OIL, 3. GAS OIL, 4. LOW TEMPERATURE TAR, 5. COAL OIL.

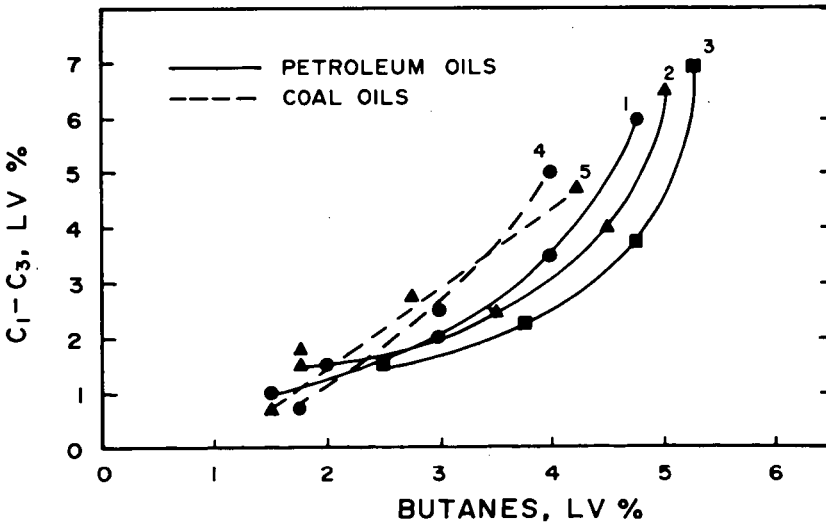


FIGURE 8. RATIO OF BUTANES AT DIFFERENT LEVELS OF NAPHTHAM YIELD.
 1. STOVE OIL, 2. DIESEL OIL, 3. GAS OIL, 4. LOW TEMPERATURE TAR, 5. COAL OIL.

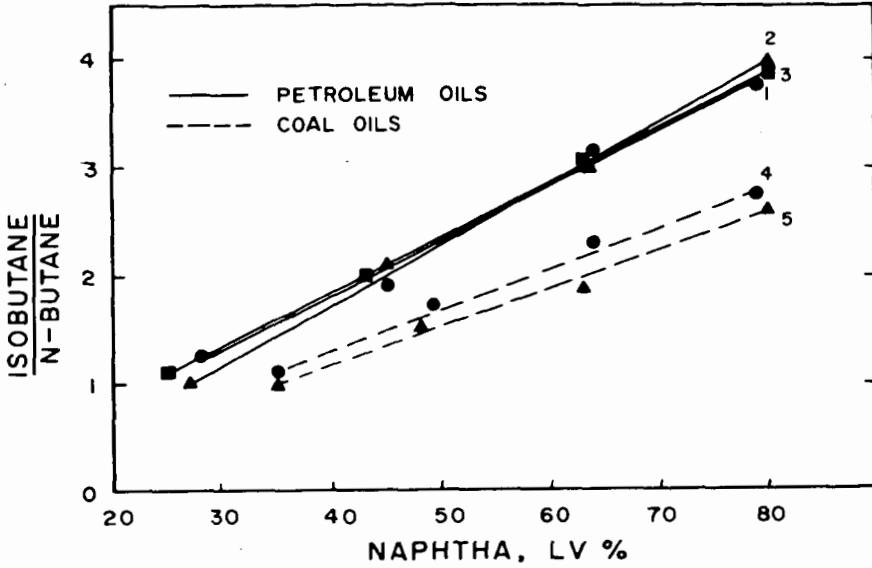


FIGURE 9. RELATIONSHIP BETWEEN THE FORMATION OF C_1-C_3 HYDROCARBONS AND BUTANES.
1. STOVE OIL, 2. DIESEL OIL, 3. GAS OIL, 4. LOW TEMPERATURE TAR, 5. COAL OIL.

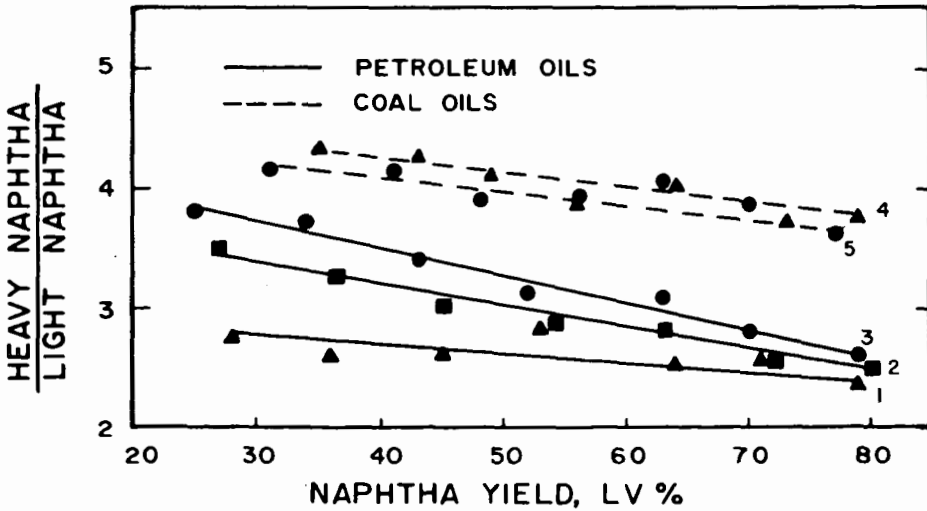


FIGURE 10. RATIO OF LIGHT AND HEAVY NAPHTHA AT DIFFERENT LEVELS OF CONVERSION.
1. STOVE OIL, 2. DIESEL OIL, 3. GAS OIL, 4. LOW TEMPERATURE TAR,
5. COAL OIL.

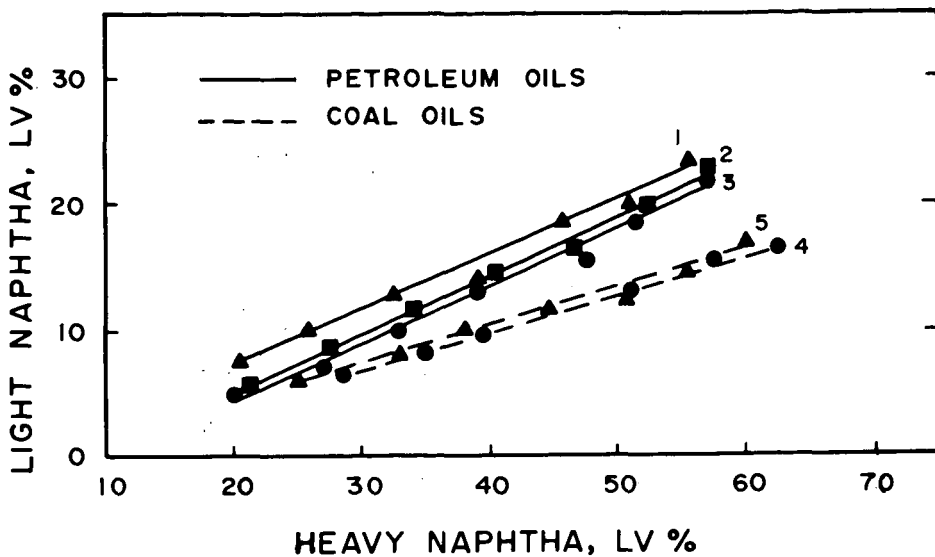


FIGURE 11. RELATIONSHIP BETWEEN THE FORMATION OF LIGHT AND HEAVY NAPHTHA.
 1. STOVE OIL, 2. DIESEL OIL, 3. GAS OIL, 4. LOW TEMPERATURE TAR,
 5. COAL OIL.

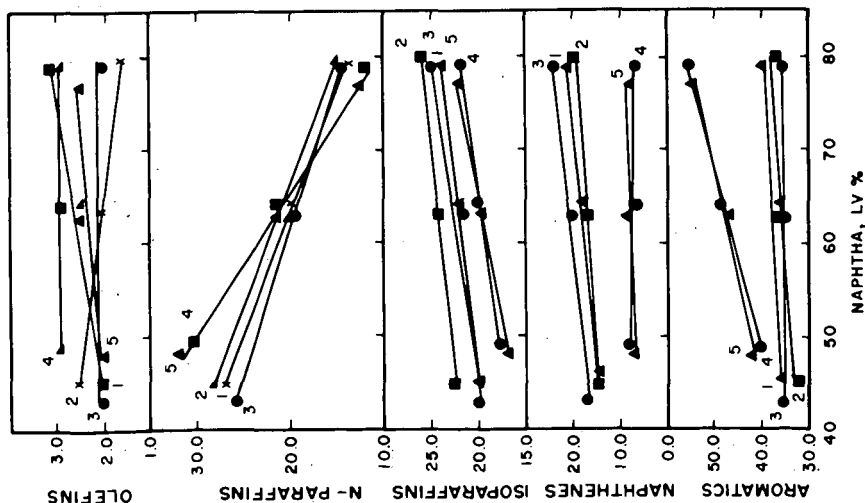


FIGURE 12. COMPOSITION OF NAPHTHA AT DIFFERENT LEVELS OF FORMATION.
 1. STOVE OIL, 2. DIESEL OIL, 3. GAS OIL, 4. LOW TEMPERATURE TAR, 5. COAL OIL.

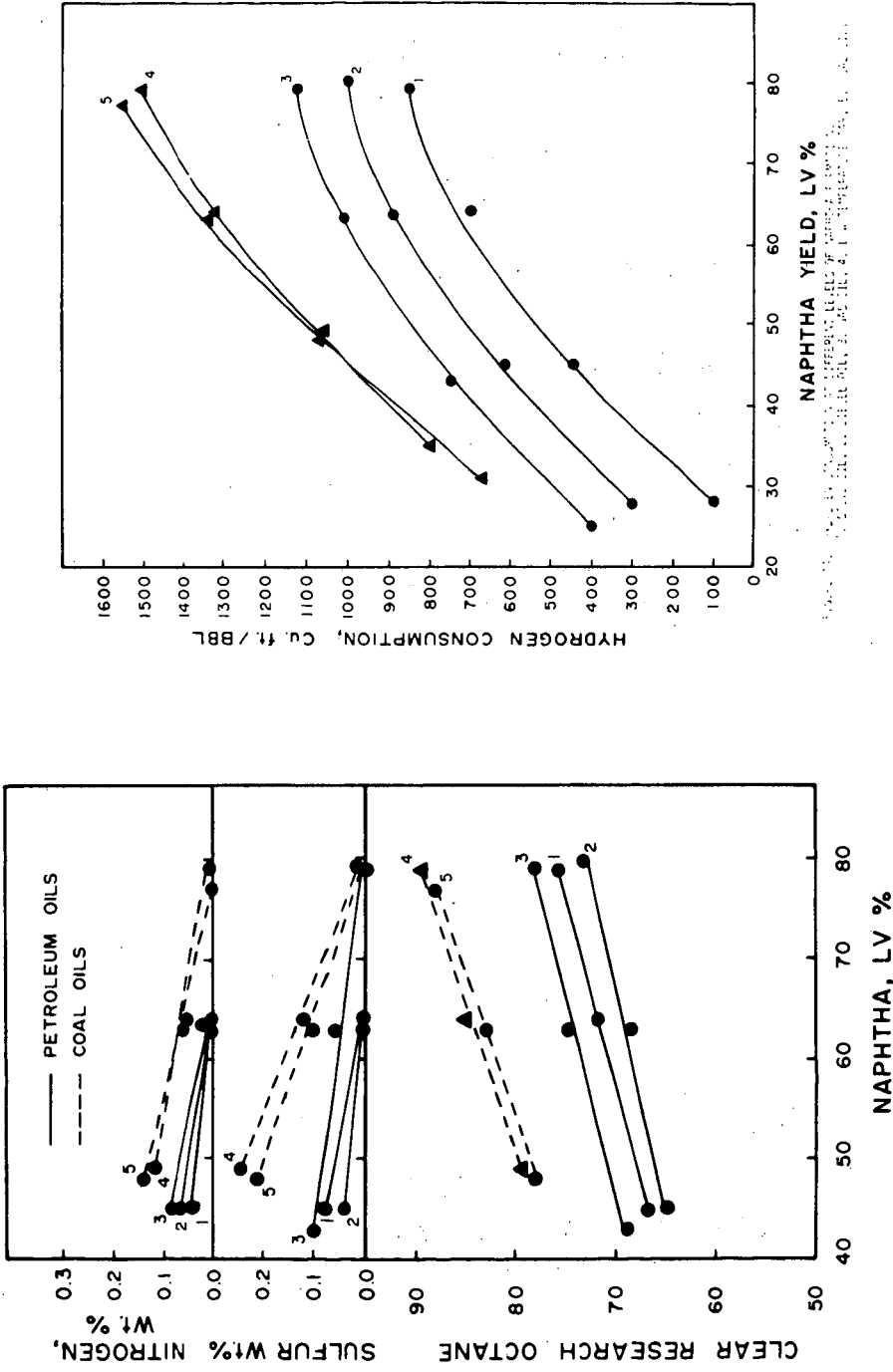


FIGURE 13. QUALITY OF NAPHTHA AT DIFFERENT LEVELS OF FORMATION.
 1. STOVE OIL, 2. DIESEL OIL, 3. GAS OIL, 4. LOW TEMPERATURE TAR, 5. COAL OIL.

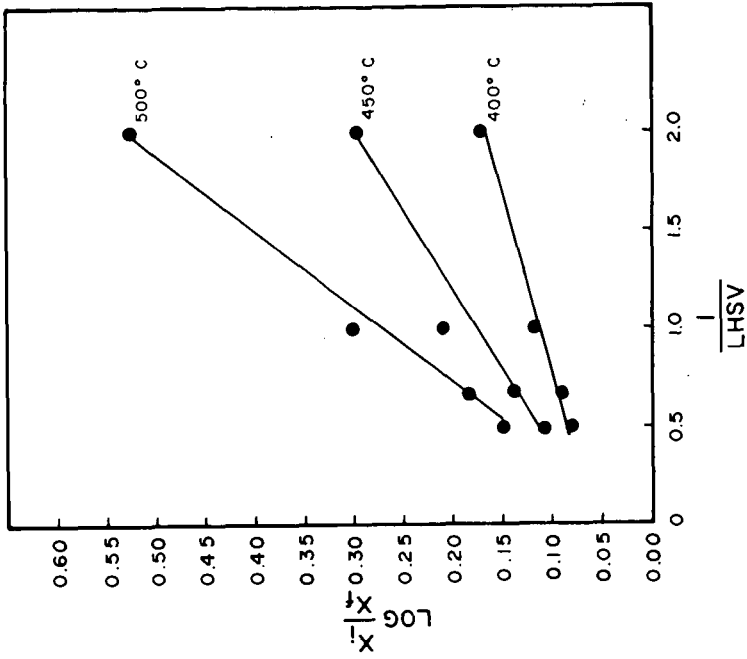


FIGURE 15. FIRST-ORDER PLOT FOR HYDROCRACKING OF BAS OIL.

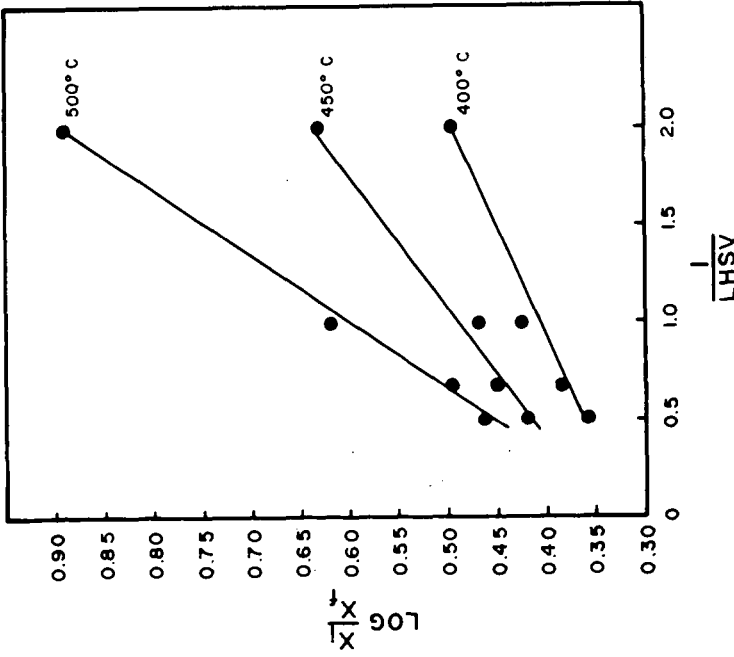


FIGURE 16. FIRST-ORDER PLOT FOR HYDROCRACKING OF COAL OIL.

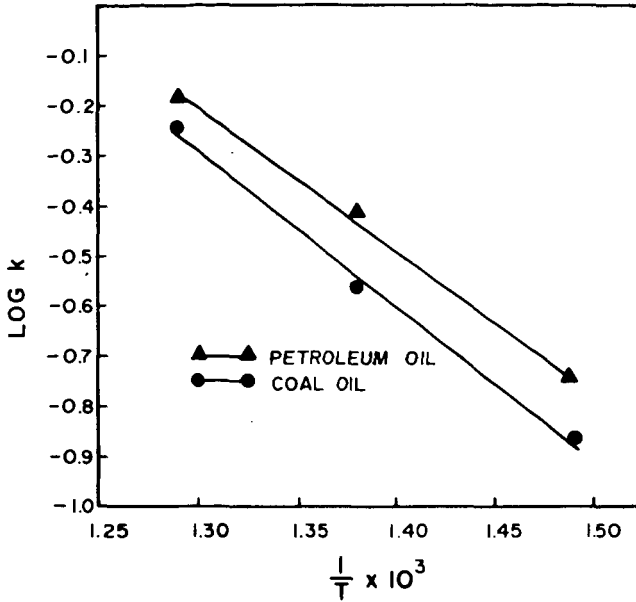


FIGURE 17. ARRHENIUS PLOT FOR HYDROCRACKING OF GAS OIL AND COAL OIL.

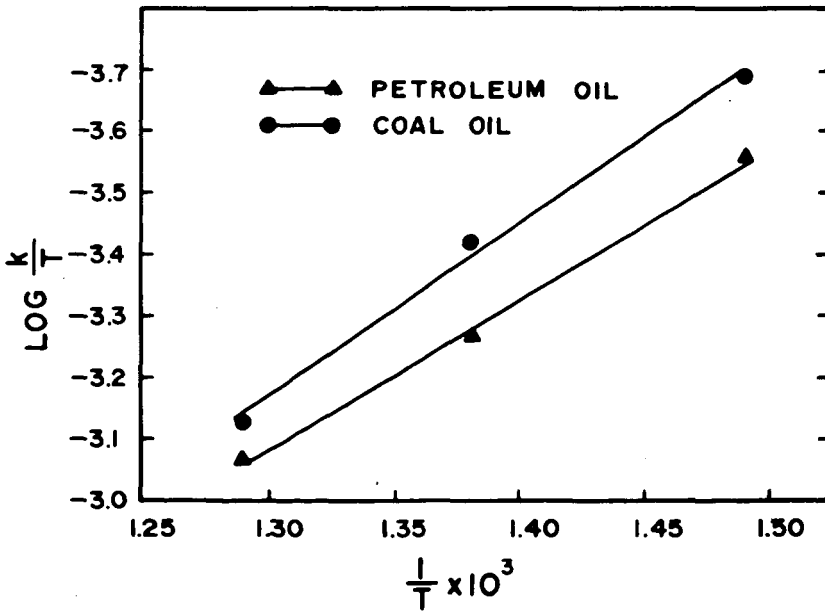


FIGURE 18. EYRING PLOT FOR HYDROCRACKING OF GAS OIL AND COAL OIL.

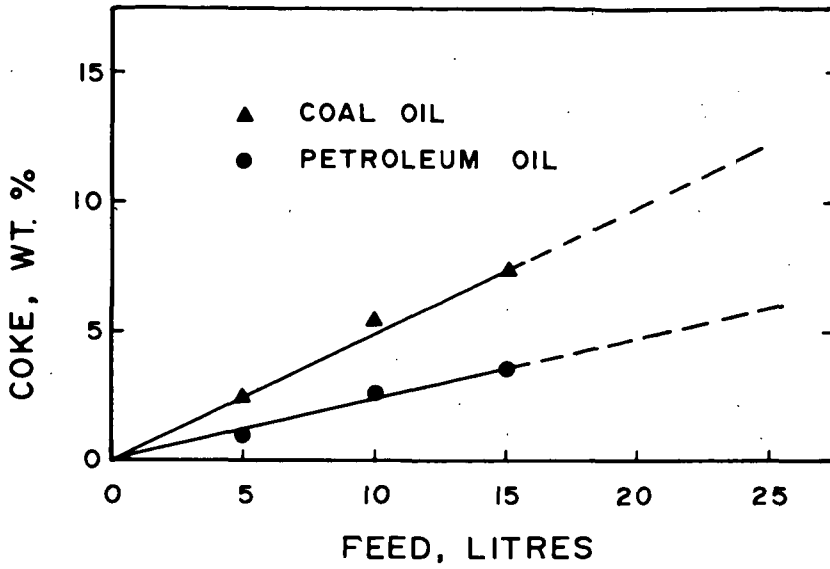


FIGURE 19. COKE FORMATION DURING HYDROCRACKING OF GAS OIL AND COAL OIL.

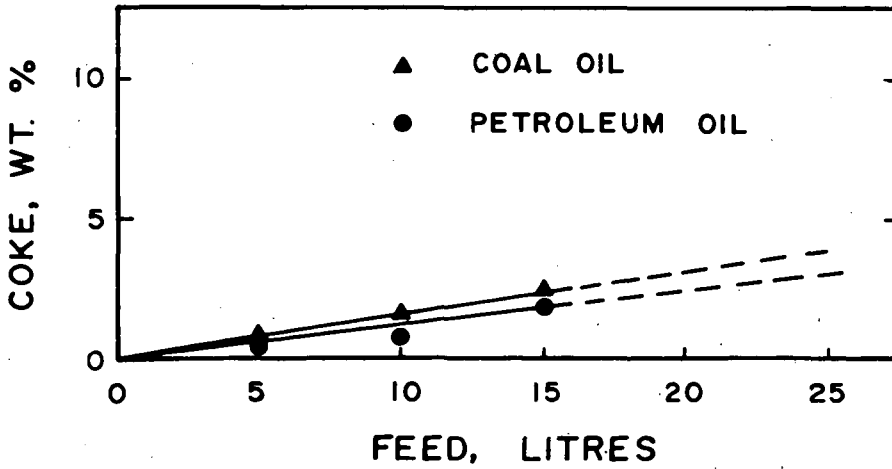


FIGURE 20. COKE FORMATION DURING HYDROCRACKING OF REFINED GAS OIL AND COAL OIL.

CONTINUOUS RAPID CARBONIZATION OF POWDERED COAL BY ENTRAINMENT:
RESPONSE SURFACE ANALYSIS OF DATA

by

John J. S. Sebastian, Robert J. Belt, and John S. Wilson

Morgantown Coal Research Center, Bureau of Mines
U.S. Department of the Interior, Morgantown, W. Va.

INTRODUCTION

In recent years increased interest in processes for converting coal into high-Btu pipeline gas and smokeless low-sulfur char for powerplants prompted the Morgantown Coal Research Center to study the rapid or flash carbonization of bituminous coal. The coal selected for carbonization was a strongly caking, high-volatile A bituminous from the Pittsburgh bed (34.4% V.M., 7.0% ash).

Of primary interest has been the development of a low-cost process for carbonizing high-volatile bituminous coals at high throughput rates in entrainment. Previously proposed low-temperature entrainment processes (1)¹, as well as our prior low temperature-entrainment carbonization work² in an externally heated 9-foot-long 4-inch-diameter isothermal reactor, yielded a high-Btu gas and a highly reactive char, along with a high yield of tar plus light oil. However, coal throughput rates were prohibitively low owing to dilute phase operation--0.35 g of coal per cu ft gas volume. Projection of such data to a commercial-scale process would result in excessively large equipment and high operating costs, although the throughput per unit cross sectional area would increase to some extent with larger carbonizers operated at higher pressures.

Dense phase entrainment, on the other hand, offered the prospect of a significant increase in coal throughput. Hence, experiments were conducted with a 4-inch-diameter by 1-foot-long carbonizer at higher temperatures with 20 times the coal concentration. The objective of this work was 3-fold: (1) to determine the effects and interactions of process variables as a guide to process feasibility; (2) to evaluate external and internal methods of applying the heat required for carbonization; and (3) to obtain data for the design of a pilot-scale carbonizer.

This paper describes these experiments, including the main steps in applying a 3-factor 5-level response surface analysis of the factorially designed test-runs, a technique that evaluates all of the significant process variables with a minimum of experimental work. Two of the 13 responses, char yield and percent volatile matter in the char, are discussed in detail.

DESCRIPTION OF EQUIPMENT

The equipment for the two test series differed in the method of heating the carbonizer and in most of the product recovery system, as shown in figures 1 and 2. The coal-feeding system was identical in both series and consisted of a vibratory screw feeder receiving coal from a pressure-equalized hopper. The feeding

¹Underlined numbers in parentheses refer to items in the list of references at the end of the paper.

²The results of these preliminary investigations will be summarized in a forthcoming U.S. BuMines Report of Investigations.

in each case was facilitated by injection of the coal into nitrogen in different dilutions with methane, before entering the flash carbonizer.

The carbonizer consisted of a 12-inch length of 4-inch-diameter, schedule 40 pipe made of type 310 stainless steel. For the external heating series, three 4-inch-long circular thermoshell heating elements were installed around the carbonizer tube. The coal particles were carbonized while being carried downward by the entraining gas. For internal heating, natural gas was burned with a slight deficiency of air in a refractory-filled combustor, the hot combustion products being injected directly into the carbonizer. The 70 percent through 200-mesh coal was further entrained in the hot gases which provided the required heat for carbonization. Internal heating changed the heat transfer from radiation controlled to turbulent convective, although some external heating was also applied to balance the heat losses from the carbonizer.

Because of the different gas flow rates for the two test series, the product recovery trains were different. In each case, the objective was complete recovery from the gas stream of all solid and liquid products. In both cases, coarser char particles fell directly into a char receiver below the carbonizer. For the externally heated unit, where the gas flow rate was lower, a baffled knockout chamber was used to remove the fine char particles. Tar and pitch were removed by two electrostatic precipitators, followed by a dry-ice trap for removal of light-oil and water, and a silica gel trap for final recovery of light-oil and water before metering and venting the gas. For the internally heated unit, which received much larger gas volumes from the combustor, the recovery train consisted of two cyclones in series for the removal of char dust, and a water scrubber followed by a steam-water scrubber for final tar, pitch, and light-oil removal.

The carbonizer was designed to rapidly heat coal particles at atmospheric pressure as they passed through the 12-inch hot zone. The feed tube was constructed to inject the powdered coal at a high velocity into the carbonization zone. After less than one second residence time, during which the particles are rapidly pyrolyzed and devolatilized, the char particles carried by the gas enter the recovery train.

In a typical test-run the carbonizer is preheated to the desired wall temperature. When the carbonizer temperature becomes constant at the desired level, the coal feeding is begun to start the run. During the run, char is periodically removed from the bottom lock hopper and the gas is sampled. All other products are collected after the run and a period of cooling.

EXPERIMENTAL DESIGN

To evaluate the data, the "composite factorial design" method (2) was used to obtain, in the least time, the best reliable estimates of the effects and interactions of system variables. Several of these variables, called "factors", were systematically changed and the effects in each case determined by statistical analysis.

A 3-dimensional coordinate system was assumed with three factors--coal-feed rate, reactor wall temperature, and entraining gas composition³--changed simultaneously while all other variables were held constant. Within this 3-dimensional

³Methane is the chief component of carbonization gases and was used in order to simulate the entrainment of coal in recycle gases as would be done in pilot-scale and commercial carbonizers. Entraining gas composition is expressed in terms of methane-to-nitrogen ratios.

system, a range of values in each operating variable was chosen for examination, based on actual results. The effects and interactions of these three factors at various levels were determined on two types of responses, product-yield and quality.

The composite factorial design allowed detailed examination of the responses at 14 points plus five replications at the center of the cube, from which the entire response surface was derived. The computation of variances was based on these five replications. The three factors were varied in an established pattern as shown in table 1 and figure 3. In these illustrations, for convenience, the factors are identified as x_1 (reactor wall temperature), x_2 (coal-feed rate) and x_3 (gas composition). The levels in each factor were coded into five values: -2, -1, 0, 1, 2. The operating factors and corresponding experimental results obtained are summarized in table 2.

The main steps in response surface analysis follow:

1. Design the experiment to obtain a second degree regression equation,
2. Transform this equation into its standard or canonical form,
3. Illustrate it by means of a contour diagram or 3-dimensional model.

Assuming that a second degree equation with three factors represents the system adequately, it will have the following general form:

$$y = b_0 x_0 + b_{11} x_1^2 + b_{12} x_1 x_2 + b_{13} x_1 x_3 + b_1 x_1 + b_{22} x_2^2 + b_{23} x_2 x_3 + b_2 x_2 + b_{33} x_3^2 + b_3 x_3 \quad (1)$$

where $b_0 x_0$ represents the average value of all trials. This equation contains a linear term and a quadratic term for each factor and all possible 2-factor interactions. The coefficients are calculated from the data.

TABLE 1. - Composite factorial design

Factors	Level					Symbol
	-2	-1	0	1	2	
Temperature.....°F	1,500	1,600	1,700	1,800	1,900	x_1
Feed rate.....g/hr	250	500	750	1,000	1,250	x_2
Gas composition.....%	100 N ₂	75	50	25	0	x_3
	0 CH ₄	25	50	75	100	

Note: Constants: (1) Coal type--Pittsburgh-bed hvAb, 34.4% V.M., 7.0% ash (dry basis).
 (2) Coal size--70 percent through 200 mesh.
 (3) Entraining gas rate--10.0 scfh.

Responses:

- | | | |
|---------------------------------|------------------------------|------------------------|
| (1) Char yield. | (5) Sulfur per Btu. | (9) Gas heating value. |
| (2) Char heating value. | (6) Percent volatile matter. | (10) Gas fuel value. |
| (3) Char fuel value. | (7) Percent sulfur. | (11) Light-oil yield. |
| (4) Extent of devolatilization. | (8) Gas yield. | (12) Tar yield. |
| | | (13) Pitch yield. |

TABLE 2. - Summary of data

Coded coordinates	Operating variables			Experimental results			
	Temp., °F	Feed rate, g/hr	Gas comp., % CH ₄	External heating		Internal heating	
				% V.M.	Char yield, lb/ton	% V.M.	Char yield, lb/ton ¹
-1 -1 -1	1,600	500	25	23.83	1,521	15.46	1,029
-1 -1 1	1,600	500	75	25.73	1,556	15.02	1,048
-1 1 -1	1,600	1,000	25	30.11	1,732	24.81	1,253
-1 1 1	1,600	1,000	75	28.91	1,719	20.56	1,178
1 -1 -1	1,800	500	25	24.20	1,433	13.74	1,030
1 -1 1	1,800	500	75	23.20	1,454	16.01	1,074
1 1 -1	1,800	1,000	25	25.71	1,513	20.85	1,221
1 1 1	1,800	1,000	75	26.07	1,619	19.76	1,194
0 0 0	1,700	750	50	26.56	1,635	14.74	1,088
0 0 0	1,700	750	50	27.76	1,589	17.11	1,117
0 0 0	1,700	750	50	28.55	1,642	18.83	1,138
0 0 0	1,700	750	50	28.96	1,638	16.62	1,060
0 0 0	1,700	750	50	28.28	1,604	15.27	1,037
-2 0 0	1,500	750	50	31.18	1,721	23.35	1,246
2 0 0	1,900	750	50	24.65	1,468	12.05	983
0 -2 0	1,700	250	50	22.58	1,305	11.99	960
0 2 0	1,700	1,250	50	31.94	1,729	16.38	1,010
0 0 -2	1,700	750	0	29.61	1,661	16.96	1,115
0 0 2	1,700	750	100	28.90	1,593	16.32	1,000

¹The low char yields from internal heating are attributable to some carry-over of fine dust into tar and pitch.

Since the regression equation is difficult to interpret, it is transformed into its standard or canonical form. The transformation is orthogonal and consists of translation of the original center of the design to the stationary point (where the slope with respect to all factors is zero) and rotation of the axes. Translation eliminates the linear terms; rotation causes the interactions to vanish. The transformed equation has the following general form:

$$Y - Y_0 = B_{11}X_1^2 + B_{22}X_2^2 + B_{33}X_3^2 \quad (2)$$

where Y_0 is the response at the stationary point and the X_1 's are the coordinates with respect to the new axes after translation and rotation.

The magnitude and signs of the coefficients in the canonical equation show the nature of the response surface. If all signs are positive, the value of the response is increasing in any direction from Y_0 , and Y_0 has a minimum value; if all signs are negative, the value of the response is decreasing, and Y_0 has a maximum value; if both positive and negative signs are present, the surface is "saddle" shaped (i.e., a ridge connecting two elevations) and there is no single maximum or minimum.

The transformation is straightforward and is based on sound mathematical procedures. The two equations, empirical and canonical, do not differ except for the location of the reference point.

All of the regression equations as well as the canonical forms have been programmed in FORTRAN IV language for the determination of the coefficients by an IBM 7040 Computer, and for plotting of the responses by an accessory CALCOMP plotter.

RESULTS

Analysis of the data by composite factorial design yields empirical equations describing the response surfaces in terms of the factors and their interactions. The coefficients of the equations indicate by their relative magnitudes the significance of the factors and the extent of their interactions as well as the curvature of the surfaces. From the equation, both linear and quadratic effects can be assessed.

The response surfaces for char yield in the external heating series are described by the regression equation:

$$y/10^3 = 1.603 - .0044x_1^2 - .0161x_1x_2 + .0131x_1x_3 - .0634x_1 \quad (3)$$

$$- .0238x_2^2 + .0046x_2x_3 + .0917x_2$$

$$+ .0037x_3^2 + .008x_3$$

The coefficients of the linear terms, $0.0634x_1$ and $0.0917x_2$, are larger than any others, thus these linear effects have the greatest significance on the char yield. Statistical analysis of the data indicates that these two factors, temperature and feed-rate, are the only significant ones at the 95 percent confidence level. Based on a similar equation for the internal heating series, the char yield response is significantly dependent only upon the coal-feed rate. In absolute magnitude, these coefficients are small, indicating that the surfaces have only a slight curvature within the limits of the experiment.

The canonical equation for char yield in external heating is:

$$Y - 1,974 = -27.4X_1^2 - 4.7X_2^2 + 7.5X_3^2 \quad (4)$$

The form of this equation indicates that the surface is saddle-shaped since both positive and negative terms appear. The stationary point in this case is an inflection point in the surface, (i.e., neither a maximum or a minimum), and since it occurs outside the experimental limits, any description of the behavior of the surface near the point is meaningless. The saddle-shaped surface indicates only a trend in the data. Figures 4 and 5 present a comparison of the shapes of the surfaces for yields of char produced by external and internal heating, respectively.

Similarly derived from another regression equation, the 3-dimensional diagrams in figures 6 and 7 show the response surfaces for volatile matter in the char, resulting from external and internal heating, respectively. Both sets of surfaces are saddle-shaped as were those for char yield. The results of the computed data (table 3) show that the surfaces for percent volatile matter in the char depend only on coal-feed rate in the case of internal heating. With external heating, both temperature and coal-feed rate have significant effects. Table 3 also summarizes the results for the four responses discussed above.

Figure 8 shows the quantitative relationship between char yield and coal-feed rate for both the internal and external heating series. In this diagram, the wall temperature of the carbonizer and the percent volatile matter in the char are shown as parameters. The solid curves represent the char yield as a function of the coal-feed rate at the temperature levels shown. The broken lines represent similarly a functional relationship between char yield and coal-feed rate, but with percent volatile matter as a parameter at the levels shown. The diagram also shows the percent volatile matter in char as a function of the coal-feed rate at given

carbonization temperatures. This follows from the fact that the char yield is a function of coal-feed rate at any carbonization temperature, as stated above.

TABLE 3. - Results of factorial analysis:
yield and quality of the char produced

Response	Significant factors ^{1,5}	Best value of response ²	Conditions yielding best response value ³	Variance accounted for ^{4,5}	Heating Method
Char yield	Temperature, feed rate	Maximum at 15% V.M. in char	Low temperatures; high feed rates; CH ₄ in gas	98.5	External
Percent volatile matter in char	Temperature, feed rate	15%	Low temperatures; low feed rates; gas composition immaterial	84.8	External
Char yield	Feed rate	Maximum at 15% V.M. in char	Low temperatures; low feed rates (250-500 g/hr); low %CH ₄ in gas	92.4	Internal
Percent volatile matter in char	Feed rate	15%	Surface extending from low temp.--low feed rate to high temp.--high feed rate	83.1	Internal

¹ Factors causing systematic variation in response.

² Desired value of response from process standpoint.

³ Values of variables (factors) required to give the desired response.

⁴ Percentage of random error accounted for in the experiment (below 80% validity of the result is poor.)

⁵ At 95% confidence level.

The factorial design indicates that both temperature and coal-feed rate are significant factors at the 95 percent confidence level in the external heating series, while only the coal-feed rate is significant at the 95 percent level in internal heating. The diagrams in figure 8 reflect these conclusions. The larger effect of temperature in the external series is seen from the greater spread between the curves compared with the set of curves for internal heating. The effect of temperature is clearly present in the internal heating series, but at a much lower statistical level of confidence.

The diagrams in figure 8 show that for a given coal-feed rate, the char yield decreases with increasing carbonization temperatures, as would be expected. However, the effect of the coal-feed rate on the char yield, at higher feed rates, is contrary to what one would expect: the char yield decreases as the feed rate increases. The observed deviation in curvature can be explained by the method used to measure temperature. When the temperature of the reactor wall is measured, as in this investigation, there is a direct correlation between the true temperature of the suspended solid particles and the measured wall temperature as long as the particles are in dilute phase in the moving gas stream. However, above a certain particle concentration the correlation between wall temperature and particle temperature ceases because the particles moving downward in dense phase near the center of the carbonizer tube will not "see" as much of the source of radiant heat as the particles moving near the tube wall. In the externally heated carbonizer, this shadowing effect becomes so large that the wall temperature is no longer a true

measure of the actual temperature. The same effect is confirmed by noting the percent volatile matter remaining in the char. Since the same coal is used throughout, the amount of volatile matter remaining in the char that is carbonized in dilute phase is directly related to the char yield. At high coal-feed rates in the external heating series, the curves representing the percent volatile matter in the char drop significantly with increasing coal-feed rate, also indicating that the linear relationship between wall temperature and carbonization temperature has ceased.

Differences in char yield and percent volatile matter remaining in the char for both series are evident from the diagram discussed. The upper plot shows that the minimum volatile matter left in the char from the external heating series was approximately 20 percent, or 5 percent above the 15 percent considered optimum for coal-burning powerplants. The optimum of 15% V.M. could not be attained by means of external heating over the entire range of factor levels investigated. On the other hand, the lower group of curves for the internal heating series indicate that 15 percent V.M. char can be made (with an entraining gas composition of 50 percent N_2 and 50 percent CH_4) at any temperature within the design limits of 1,500° to 1,900°F, and at coal-feed rates from 375 to 750 g/hr. The corresponding char yield was 1,075 lb per ton of coal carbonized.

A complete description of the yields and qualities of all of the products (including gas, light oil, tar and pitch) will be included in a forthcoming U.S. BuMines Report of Investigations.

CONCLUSIONS

The experimental results of the two test series show that even highly caking coals may be carbonized at a rapid rate in entrainment. The quantities and qualities of the products can be controlled within the limits of the experiment by appropriately combining the temperature, coal-feed rate and entraining gas composition.

Larger coal throughput rates, with the desired amount of volatile matter remaining in the char, were possible when the carbonizer was heated internally rather than externally because of more effective heat transfer, although at the expense of gas quality. Thus, by internal heating, optimum char quality (15% V.M.) was achieved with a throughput of 750 g/hr in a 4-inch-diameter carbonizer at 1,900°F. Comparable char quality could not be attained by external heating over the entire range of the variables investigated.

Diagrams obtained by response surface analysis of the two series of test-runs were found useful in predicting the conditions under which a product of given yield and quality can be produced. Optimization of product yields and qualities could be achieved by subsequent series of factorially designed test-runs guided by the trends indicated by the present results.

REFERENCES

1. Sebastian, J. J. S. Process for Carbonizing Coal in a Laminar Gas Stream. U.S. Patent 2,955,988, October 11, 1960.
2. Davies, O. L., Ed., The Design and Analysis of Industrial Experiments. Hafner Publishing Co., N. Y., 1963.

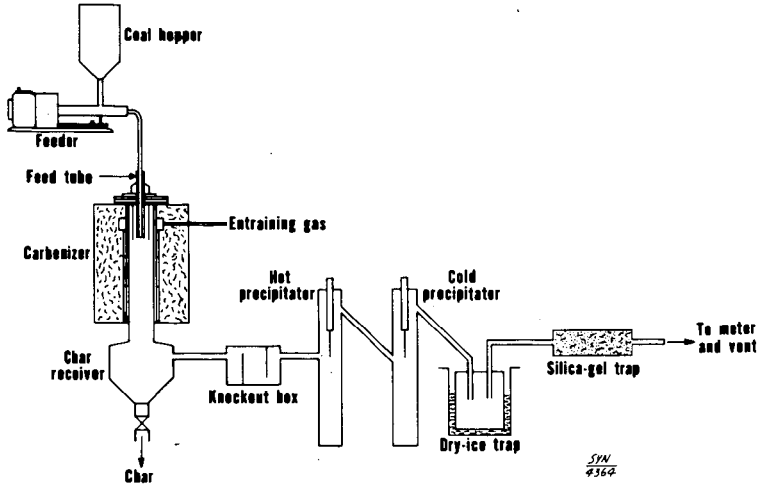


FIGURE 1. - Flash Carbonization of Powdered Coal with Externally Heated Reactor

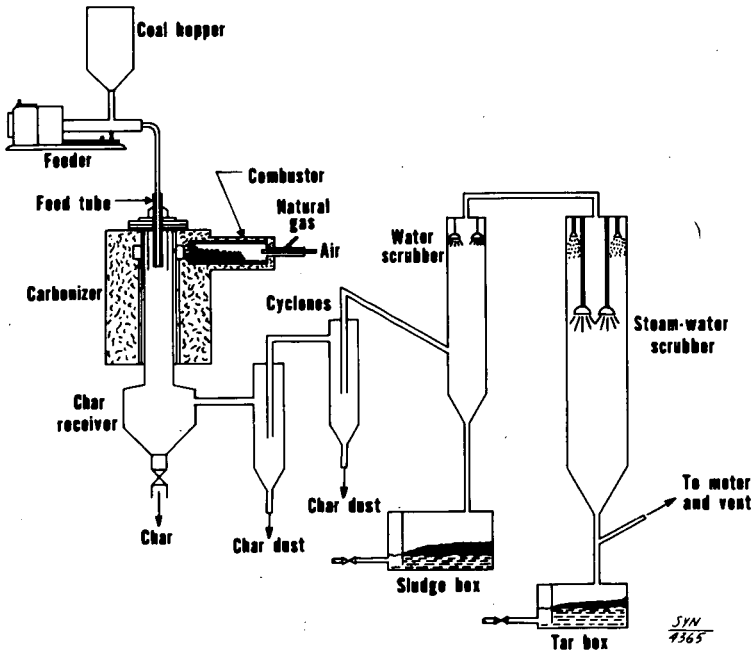
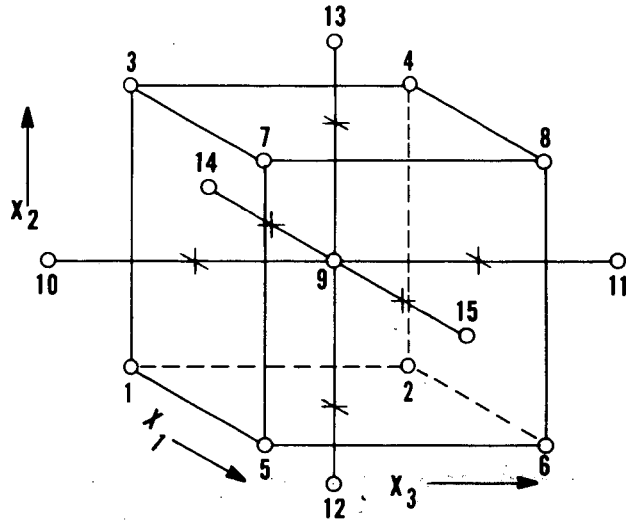


FIGURE 2. - Flash Carbonization of Powdered Coal with Internally Heated Reactor



EXPERIMENTAL
POINTS IN
CODED
COORDINANTS

POINT	X ₁	X ₂	X ₃
1	-1	-1	-1
2	-1	-1	1
3	-1	1	-1
4	-1	1	1
5	1	-1	-1
6	1	-1	1
7	1	1	-1
8	1	1	1
9	0	0	0
10	0	0	-2
11	0	0	2
12	0	-2	0
13	0	2	0
14	-2	0	0
15	2	0	0

FIGURE 3. - Three-Factor Composite Design

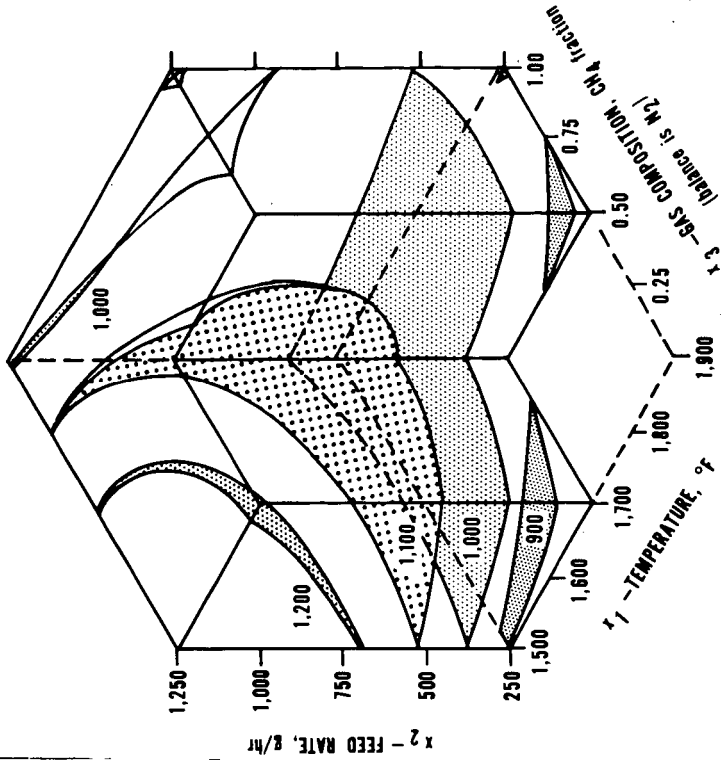


FIGURE 5. Three-Dimensional Response Surfaces, Char Yield in lbs/ton
—Internally Heated Carbonizer—

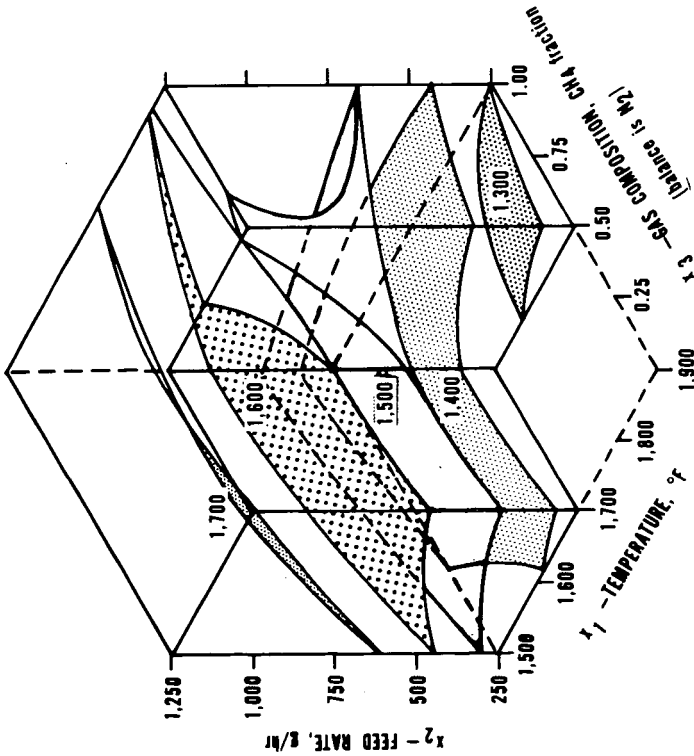


FIGURE 4. Three-Dimensional Response Surfaces, Char Yield in lbs/ton
—Externally Heated Carbonizer—

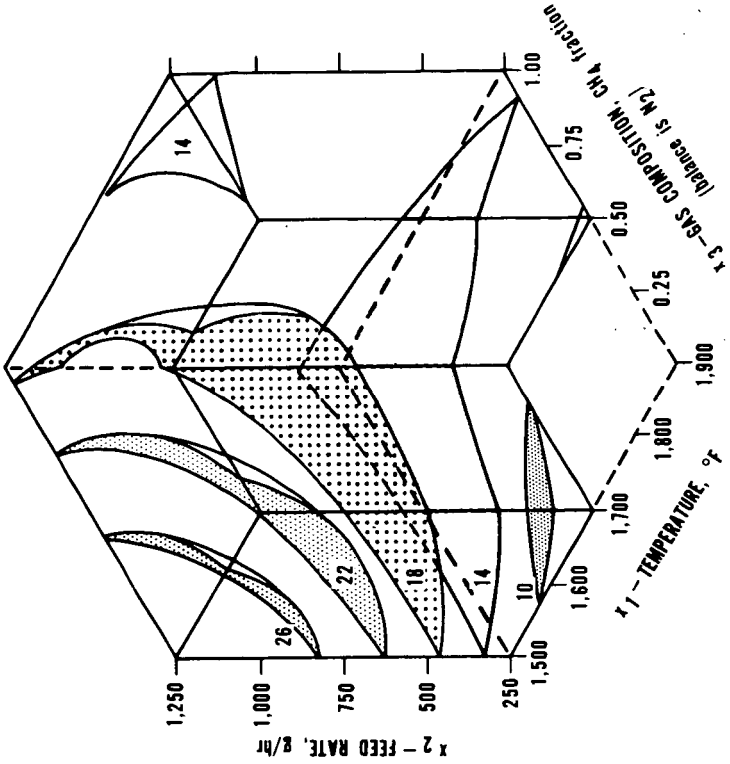


FIGURE 7. Three-Dimensional Response Surfaces, Percent Volatile Matter in Char
—Internally Heated Carbonizer—

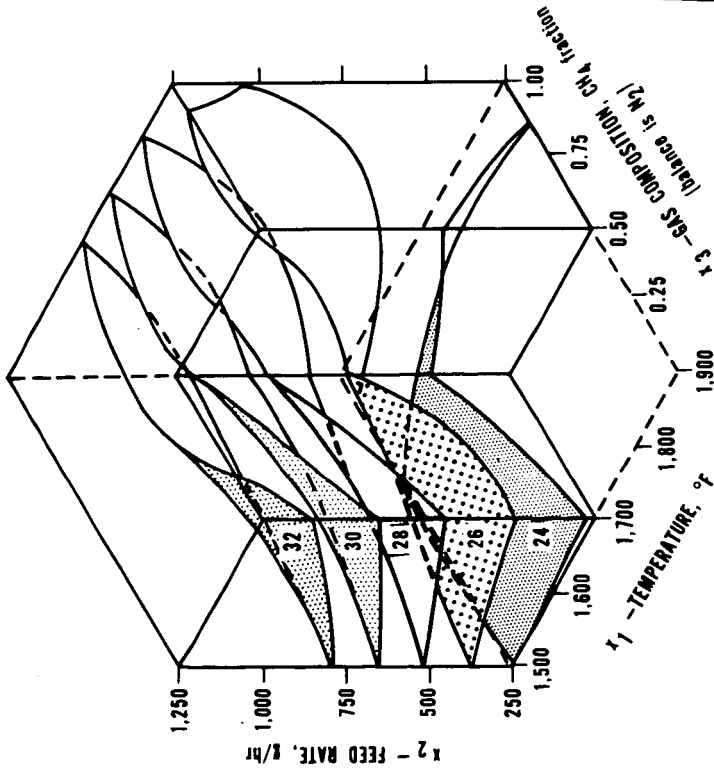


FIGURE 6. Three-Dimensional Response Surfaces, Percent Volatile Matter in Char
—Externally Heated Carbonizer—

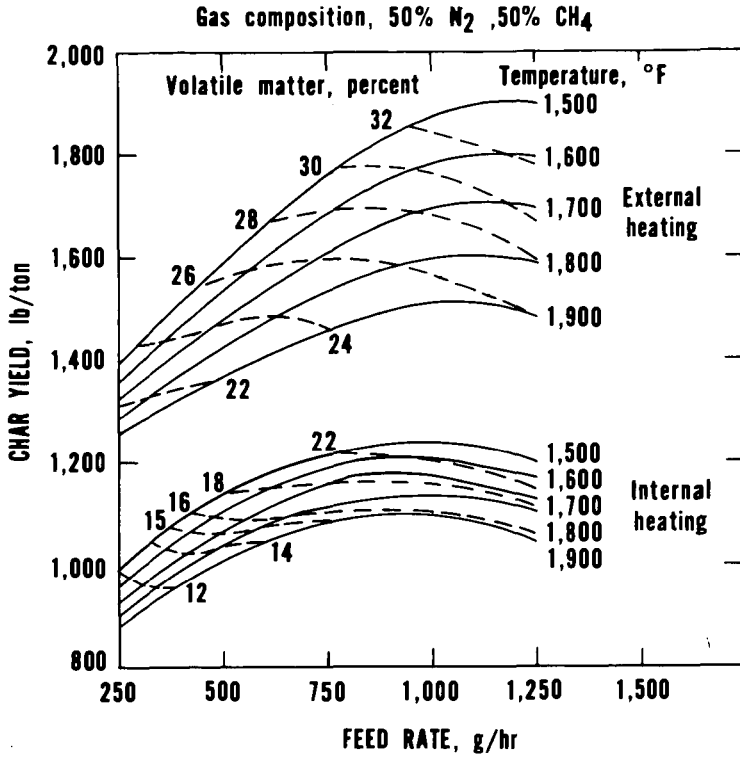


FIGURE 8. - Effect of Feed Rate and Temperature on Char Yield and Percent Volatile Matter in Char.

THERMAL CRACKING OF LOW-TEMPERATURE LIGNITE PITCH. PART II.

Richard L. Rice, Delmar R. Fortney, and John S. Berber

Morgantown Coal Research Center, Bureau of Mines,
U. S. Department of the Interior, Morgantown, W. Va. 26505

Thermal cracking of pitch from the carbonization of Texas lignite at low temperature has been under investigation as a means of producing aggregate and a binder that could be used to fabricate carbon metallurgical electrodes. A previous report on this subject covered preliminary tests on the thermal cracking of lignite pitch at 1,450° F in a 2-1/2 inch diameter reactor and showed that a variety of products could be obtained (1). In this work, a 4-inch diameter reactor was utilized to evaluate oil, coke, and gas quality and yields as a function of pitch feed rate temperature between 1,200° and 1,450° F.

EQUIPMENT AND MATERIALS

Figure 1 is a flowsheet of the system. The cracking unit consisted of a 93-inch length of 4-inch schedule 40, type 304, stainless-steel pipe, heated electrically. Total heating capacity of the cracker was 13.74 kw. A 1-inch pipe extended up through the center to within about 2-1/2 feet of the top and was perforated with 1/4-inch openings to allow withdrawal of gas and oil vapors from the reaction zone.

Pitch utilized as feed material was prepared by distilling crude low-temperature lignite tar under vacuum to an atmospheric boiling point of 660° F. The pitch yield was about 45% of the tar. Ultimate analysis and physical properties of the pitch are summarized in Table 1.

PROCEDURE

Pitch heated to 400° F was pumped from the feed tank by a gear pump through electrically heated lines into the top of the thermal cracker. Pitch utilized in all the runs came from the same source and was analyzed each time for C and H content. No significant difference was found. A flow of purge gas (11% CO₂, 88% N₂) swept products from the reaction zone. Cracked pitch was collected in the receiver and the oil was condensed and separated. Gas was passed through the scrubber and gas meter, then sampled and vented. After each run, which lasted 1-1/2 hours, the pitch flow was stopped and the pump was flushed with tar distillate fraction (from tank) to keep the pump from freezing during shutdown. It is not likely that true steady state was achieved owing to change in reactor geometry by build-up of coke. Also, heat transfer changed for the same reason. Steady state conditions are believed to have been approached, however.

After the cracking unit cooled, it was opened at the top and bottom and the coke was removed from the walls. Cracked pitch was removed from the receiver and oil was drained from the condenser and knockout. Each of the three products was weighed to the nearest one-tenth pound. The oil was distilled under vacuum to an atmospheric boiling point of 752° F, giving about 20 to 30% distillate and 70

to 80% residue. This residue was tested for carbon and hydrogen content and for softening point. If the test results were in the desired range, the residue was used as an electrode binder. The distillate was oxidized to phthalic and maleic anhydrides or separated into acids, bases, and neutral oils. The neutral oils were separated into n-olefins, paraffins, and aromatics.

Gas produced by the thermal cracking was analyzed by gas chromatography.

RESULTS AND DISCUSSION

Thermal cracking was carried out at temperatures from 1,200° to 1,450° F and pitch feed rates varying from 5.5 to 9.5 lb/hr.

A residence time (liquid basis) of nearly 0.70 second was found necessary to crack the pitch. In initial tests with a 5-foot-long cracker, the residence time was only slightly more than 0.55 second and cracking was not effected. Addition of a 2-1/2 foot length of pipe to the cracker increased the residence time to 0.68 second, an increase sufficient to crack the pitch.

Figure 2 shows the coke yield for three different feed rates at the temperatures investigated. Highest coke yields were obtained at the lowest feed rate, indicating that the lower space velocity (gas basis) led to a greater percentage of the pitch coming into contact with the hot wall of the cracker. The higher cracking temperatures also produced more coke. In the 2-1/2 inch diameter reactor that had been used before, coke yields were lower and cracked pitch yields were higher.

The oil yield, shown in Figure 3, was higher at the 5.5 lb/hr pitch rate, but a yield inversion occurred between 7.0 and 9.5 lb/hr. Thus, the oil yield decreased with increase in feed rate to a certain point, then increased. Possibly, the oil is derived by two means during the cracking process: (1) distillation of feed pitch, and (2) cracking, with the latter predominant at low rates and giving way to distillation at high rates. This seems to be verified by the decrease in carbon-hydrogen ratio of the oil residue with increase in feed rate, as shown in Figure 4. Figure 4 also shows that the carbon-hydrogen ratio of the oil residue increases with increasing temperature, this indicating the greater cracking effect of higher temperatures.

Gas yields, Figure 5, appear to have been less affected by feed rate until 1,300° F when the yields leveled out at different percentages, the leveling plateau being higher at lower feed rates. This indicates that higher cracking temperatures and longer residence time both tend to produce more gas due to the greater amount of cracking that occurs.

Typical material balances are given in Table 2. Product recovery was generally greater than 90 percent. Some losses were incurred in removing the coke from the reactor and the cracked pitch from the receiver. Material balances had been established for the system in previous experiments and were published (1). In these earlier tests, material balances ranged from 91.6 to 99.1 percent.

TABLE 2. - Material Balance for Thermal Cracking of
 Low-Temperature Lignite Pitch

Crude pitch rate, pph	Coke rate, pph	Oil rate, pph	Cracked			Total, pph	Loss, pph	Loss, pct
			pitch rate, pph	Gas rate, pph	Loss, pct			
9.0	2.5	2.5	0.8	2.6	8.4	0.6	6.7	
7.0	1.9	1.6	0.9	2.0	6.4	0.6	8.6	
9.2	2.5	2.6	0.9	2.6	8.6	0.6	6.5	
6.7	1.8	1.8	0.7	2.2	6.5	0.2	3.0	
9.5	2.7	2.7	0.9	2.7	9.0	0.5	5.2	
5.6	1.6	1.6	0.2	1.7	5.1	0.5	9.0	

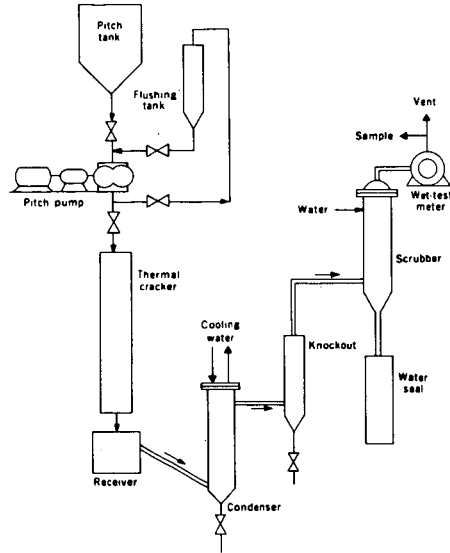


FIGURE 1. - Thermal Cracking System.

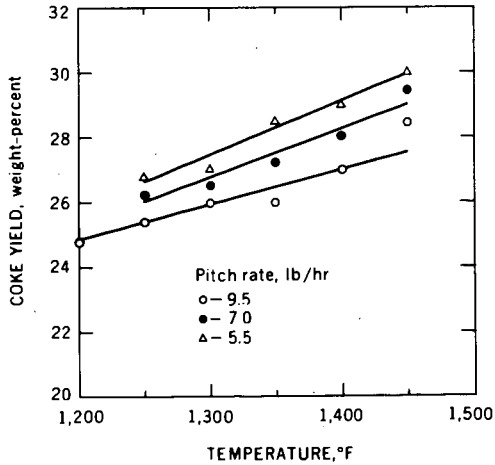


FIGURE 2. - Coke Yield as a Function of Pitch Rate and Temperature.

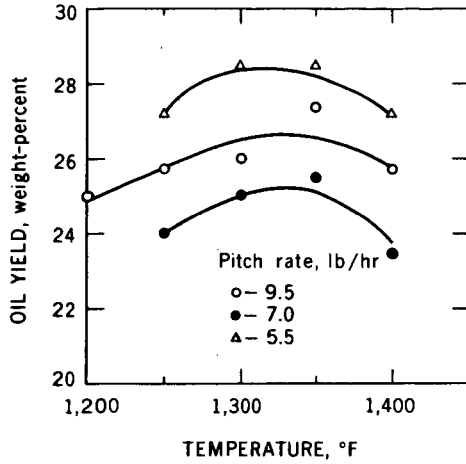


FIGURE 3. - Effect of Pitch Rate and Temperature on Oil Yield.

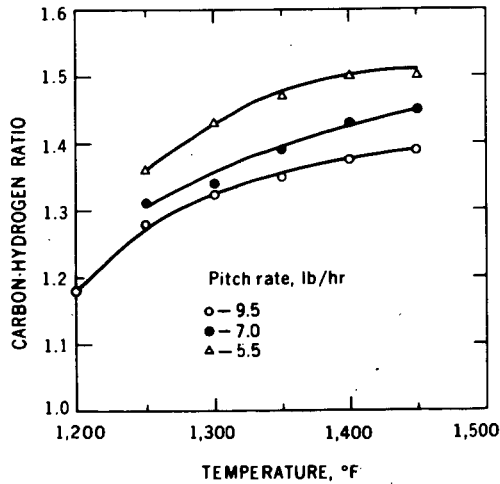


FIGURE 4. - Carbon-Hydrogen Ratio of Oil Residue.

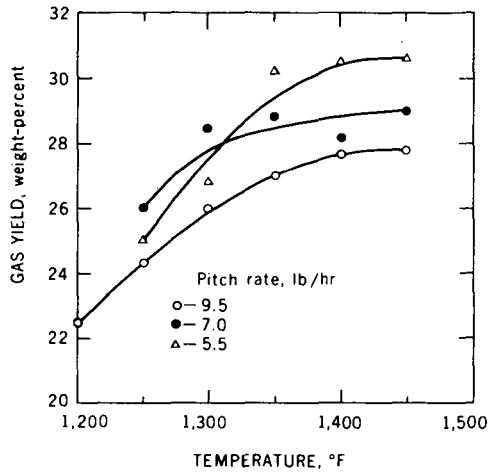


FIGURE 5. - Effect of Pitch Rate and Temperature on Gas Yield.

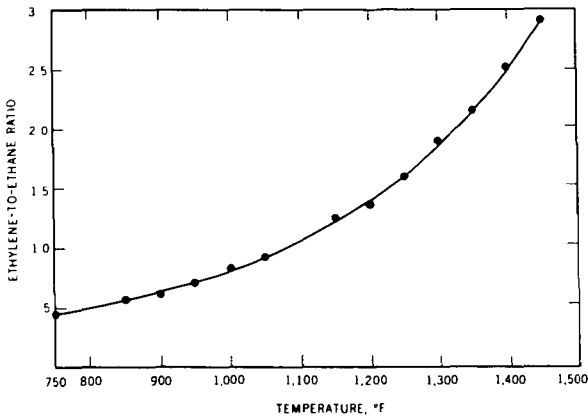


FIGURE 6. - Ethylene-to-Ethane Ratio Versus Temperature.

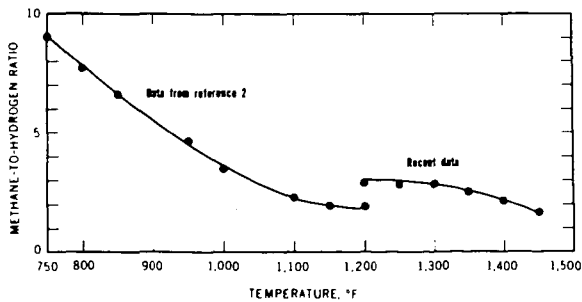


FIGURE 7. - Methane-to-Hydrogen Ratio Versus Temperature.

GAS TRANSPORT THROUGH SECTIONS OF SOLID COAL

F. S. Karn, A. G. Sharkey, Jr., B. M. Thames,
and R. A. Friedel

U.S. Department of the Interior, Bureau of Mines,
Pittsburgh Coal Research Center, Pittsburgh, Pa. 15213

ABSTRACT

Measurements were made for helium and methane flowing through thin disks of coal. Flow increased with pressure differential and temperature. At room temperature and a pressure differential of one atmosphere the flows along the bedding plane were: helium, $873 \times 10^{-10} \text{ cm}^2 \text{ sec}^{-1}$, and methane $1.2 \times 10^{-10} \text{ cm}^2 \text{ sec}^{-1}$. Flow rates were 50 percent lower across the bedding plane of the coal than along the coal seam. Activation energies were $3.9 \text{ kcal mole}^{-1}$ for helium and $13.6 \text{ kcal mole}^{-1}$ for methane for flow measured either along or across the bedding plane.

Knowing the rate at which gases will diffuse through coal will help not only in understanding reactions that can alter the properties of coal, such as oxidation, but also in studying the drainage of methane and other combustible gases from coal mines. Of all the methods of measuring diffusion, varying from the determination of massive emission from a coal-mine face to the measuring of desorption from micron-size particles, gas transport through solid coal sections appears the most promising. For the present experiments, thin disks were prepared from sections of coal cut parallel and perpendicular to the bedding planes of the coal seam. Tests with a series of disks from various locations in the same mine have shown reproducible results. Previous investigators have encountered difficulty in measuring low flow rates through solid coal. With a high sensitivity (500,000 divisions per torr) mass spectrometer we have measured the flow of methane and of helium, a reference gas, through solid sections of coal. Methane, the chief component of fire damp in a coal mine, has a very low rate of diffusion at the temperatures usually found in mines. Cervikl^{1/} has discussed the flow of gas in coal mines; flow mechanisms include diffusion through the micropore structure and permeation through the fracture system.

Laboratory-diffusion experiments reported by other investigators have been of two types. One type of experiment is the measurement of sorption or desorption on ground coal where gas penetration into the ultrafine pore structure is diffusion controlled. A second technique is the direct measurement of gas flow across a thin section--the method used in this investigation. Zwietering^{2/} and Schilling^{3/} based diffusion coefficients on methane sorption on powdered coal. Graham^{4/} and Sevenster^{5/} reported diffusion coefficients for methane flow through a thin section of coal.

Investigator	Coal form	Pressure differential, torr	Gas flow rate, $\text{cm}^2 \text{ sec}^{-1}$
Swietering ^{2/}	Powder	27	2×10^{-12}
Schilling ^{3/}	Powder	736	3×10^{-10}
Graham ^{4/}	Disk	760	15×10^{-8}
Sevenster ^{5/}	Disk	400	3×10^{-11}

Sorption methods require an estimate of surface area, path length, and frequently a temperature extrapolation. Hofer^{6/} using adsorption and Walker using desorption^{7/} reported data in terms of $\text{cm}^3\text{g}^{-1}\text{sec}^{-1}$. These data are useful for comparing gas flow at various temperatures and pressures. The data presented in this paper may be more properly defined as flow rates than diffusion coefficients. The rates are expressed as $\text{cm}^2\text{sec}^{-1}$ based on the volume of gas transported, the geometric area of the face, and the thickness of the coal disk.

EXPERIMENTAL

Our experimental procedure is a modification of the method reported by Sevenster.^{5/} Coal disks were prepared from sound coal samples selected from the Bruceston Mine in the Pittsburgh seam (hvab coal). A sample was considered sound if it had no visible cracks and if the helium flow met standards established by testing a large number of coal disks. The disks were cut and ground to 13 to 19 mm diameter and 1 to 6 mm thickness. Disks about 1 mm thick were good for pressure differentials of 20 to 120 torr, but 6 mm thickness was necessary for pressure differentials of about 1 atmosphere. The disks were prepared so that gas flow could be measured either along or across the bedding plane of the coal. Each coal disk was sealed with epoxy cement to the flared end of a glass tube which had been fused inside another glass tube (Figure 1). This established two bulbs separated by the coal disk. The bulbs were evacuated to less than 1 micron pressure over a period of 18 hours at 100° C. After evacuation bulb A was filled with helium or methane at 20 to 760 torr. Bulb B was opened at appropriate intervals and the gas analyzed by mass spectrometry. Gas flows were measured at approximately 10° C intervals between room temperature and 100° C with the temperature controlled with an electric heating jacket and thermostat. Gas flow rates were expressed as cubic centimeters (at standard conditions) of helium or methane which would pass per second through a disk 1 square centimeter in cross section and 1 centimeter in thickness ($\text{cm}^2\text{sec}^{-1}$). The pressures in the two bulbs remained essentially constant during each experiment.

The pretreatment of the coal disk strongly influenced the initial rate of gas flow. The standard pretreatment (evacuation at 100° C for 18 hours) was designed to evacuate gases from the coal-pore system without altering the coal. Gas flow through a freshly evacuated disk was rapid at first but decreased with time, and reproducible data could only be obtained after an induction period of several days. After 3 days a constant flow rate was observed. Initial flow rates varied with the extent of evacuation, but in all cases the data were reproducible after a steady flow rate was established.

RESULTS

Data were obtained for 10 disks of varying thickness and cut either along or across the bedding plane of the coal seam. Helium flows were measured both along and across the bedding planes at several temperatures between 24° and 100° C. Arrhenius plots gave activation energies of 3.9 kcal mole⁻¹ for flow in either direction. The flow rate along the bedding plane was approximately three times the rate across the bedding plane. Helium flows were measured also at a series of pressures between 4 torr and 760 torr and at room temperature. These data were extrapolated to zero flow at zero pressure drop.

Since the flow varied directly with pressure, helium flow rates could be calculated at room temperature and a pressure differential of 1 atmosphere.

Gas flows at room temperature and a pressure differential of 1 atmosphere, observed directly, have been verified by extrapolation of a series of observations at several pressures and temperatures.

	Helium flow, $\text{cm}^2\text{sec}^{-1}\text{atm}^{-1} \times 10^{10}$		
	from temperature data	from pressure data	direct
Flow along	1114	786	780
Flow across	361	325	300

In like manner methane flows were measured both along and across the bedding plane at several temperatures. Arrhenius plots (Figure 2) gave activation energies of $13.6 \text{ kcal mole}^{-1}$ for flow in either direction. Methane flow also varied with pressure (Figure 3).

Methane flow rates were obtained from three sources.

	Methane flow, $\text{cm}^2\text{sec}^{-1}\text{atm}^{-1} \times 10^{10}$		
	from temperature data	from pressure data	direct
Flow along	1.2	1.2	1.2
Flow across	0.3	1.2	0.5

DISCUSSION

The mechanism for gas flow through coal could be molecular diffusion through the small pores, bulk diffusion through the larger pores, or permeation through the fracture system of the coal bed. Zwietering and van Krevelen,^{8/} using mercury penetration, measured the pore-size distribution for a low-volatile bituminous coal and found pores varying from a few angstroms to 50,000 Å. Cervik^{1/} described the various flow mechanisms encountered in mine workings. The reproducibility between coal disks makes it unlikely that fracture porosity was encountered in the laboratory tests described in this paper. Diffusion of gases through porous solids has been described^{9/} as proportional to the concentration gradient (Fick's law) and inversely proportional to the square root of the molecular weights of the gases. This paper has confirmed the applicability of Fick's law but not the molecular weight dependence. For molecular flow helium should diffuse at twice the rate of methane; the ratios observed were 800:1 at room temperature and 40:1 at 100° C. This might be explained as diffusion modified by gas adsorption on the pore walls or by activated diffusion as suggested in references 5 and 8.

Flow along the bedding plane was faster than flow across the bedding plane. The assumption that the rate of gas transport would vary inversely with the disk thickness was supported where a disk 2.2 mm thick was compared with a disk 6.0 mm thick.

Methane flow data obtained in this study ($1.2 \times 10^{-10} \text{ cm}^2\text{sec}^{-1}\text{atm}^{-1}$ along the bedding plane, 0.7×10^{-10} across) can be compared with the value $0.28 \times 10^{-10} \text{ cm}^2\text{sec}^{-1}\text{atm}^{-1}$ reported by Senenster.^{5/} The two experiments were carried out on different coals and possibly different orientations of the bedding plane. The activation energies reported here for methane ($13.6 \text{ kcal mole}^{-1}$) and helium ($3.9 \text{ kcal mole}^{-1}$) are consistent with data in the recent literature. Kayser^{10/} measured gas sorption on a 30-percent volatile-matter coal and reported 10.9 and 2.4 kcal mole^{-1} respectively.

REFERENCES

1. Cervik, J., Mining Congress Journal, 1967, 52.
2. Zwietering, P., Overeem, J., and van Krevelen, D. W., Fuel, Lond., 1956, 35, 66.
3. Schilling, H., Juntgen, H., and Peters, W., Sixth Inter'l Conf. on Coal Science, Munster, W. Germany, 1965.
4. Graham, I., Trans. Instn. Min. Engrs., Lond., 1918, 58, 32.
5. Sevenster, P. G., Fuel, Lond., 1959, 38, 403.
6. Hofer, L. J. E., Bayer, J., and Anderson, R. B., Bureau of Mines Rept. of Investigations 6750, 1966, 13 pp.
7. Walker, P. L., and Nandi, S. P., Special Report of Research SR-42, Feb. 15, 1964, The Pennsylvania State University, University Park, Pa.
8. Zwietering, P., and van Krevelen, D. W., Fuel, Lond., 1954, 33, 331.
9. Peters, W., and Juntgen, H., Brennstoff-Chemie, 1965, 46, No. 2, 38-44.
10. Kayser, H., and Peters, U., Seventh Inter'l Conf. on Coal Science, Prague, Czechoslovakia, 1968.

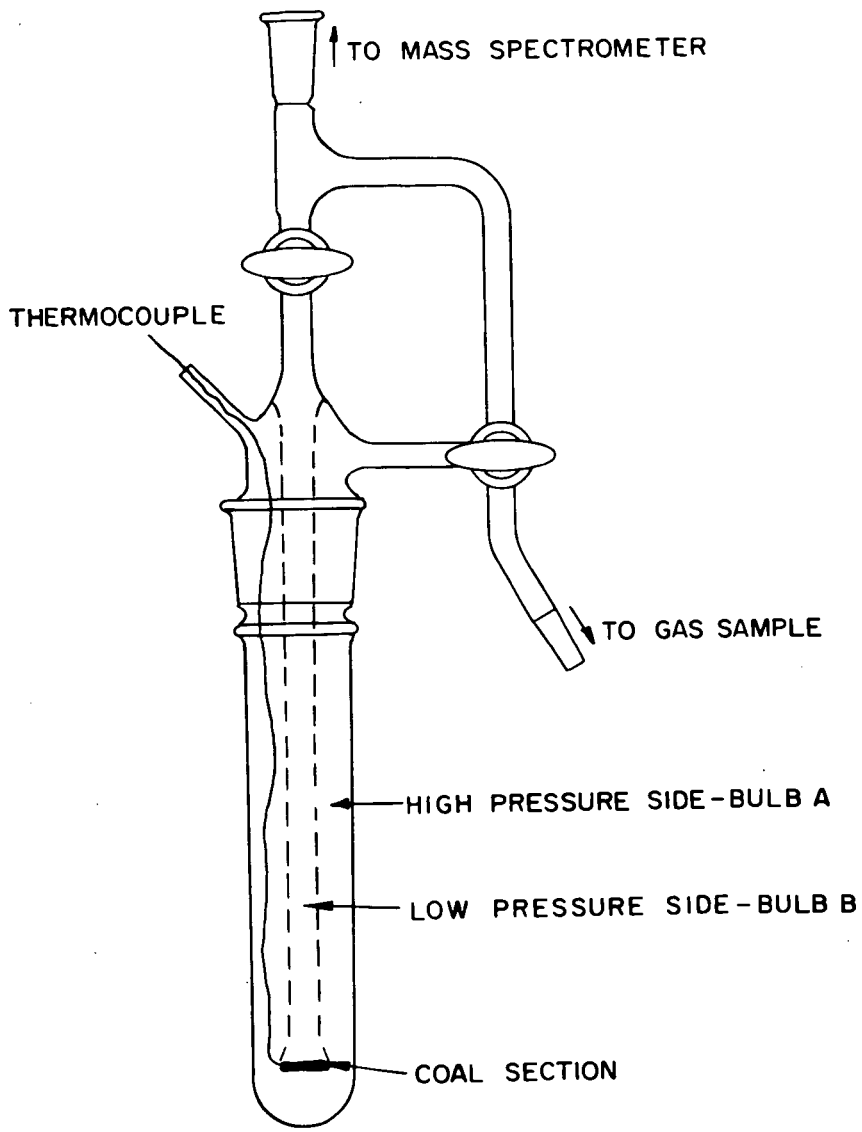


Figure 1.- Diffusion apparatus.

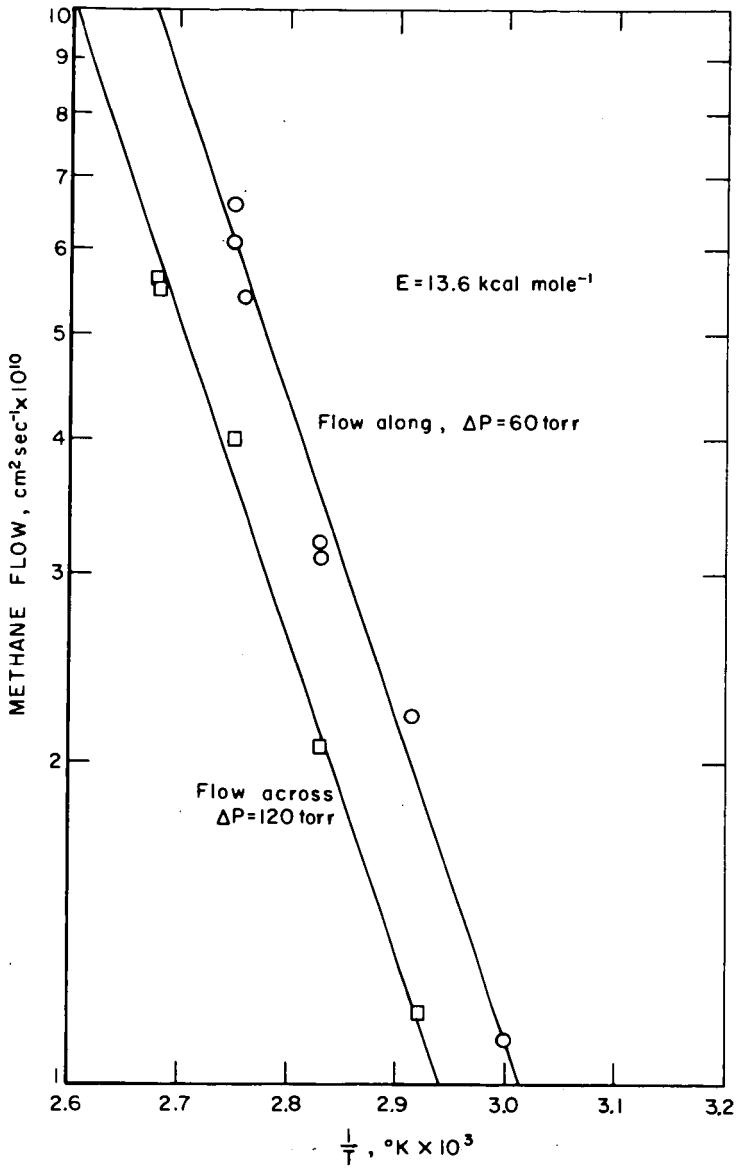


Figure 2.- Gas flow as a function of temperature. Methane flow along and across the bedding plane of Pittsburgh seam coal.

L-10760

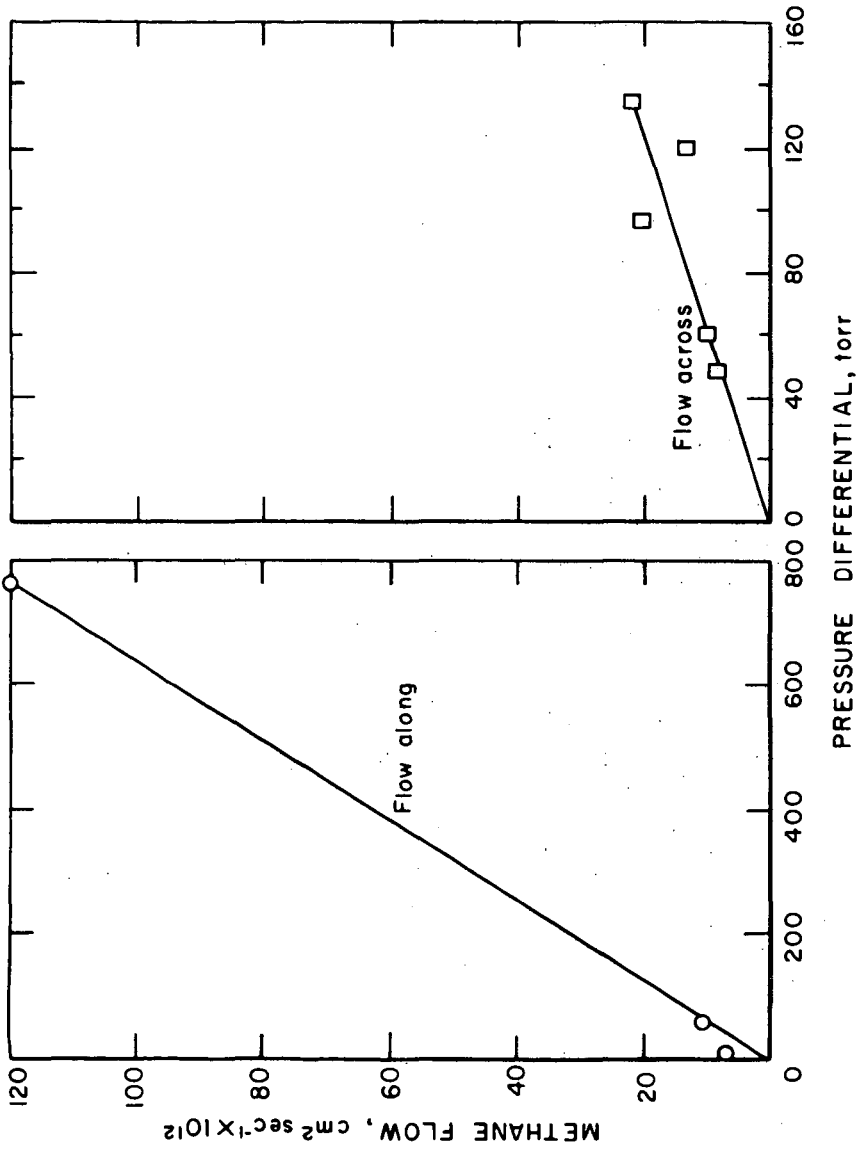


Figure 3.- Gas flow as a function of pressure differential. Methane flow along and across the bedding plane of Pittsburgh seam coal. Temperature 24° C.

The Different Effects of Flame Chemistry on the Formation
of Ethylene and the Oxides of Nitrogen in Flames

R. B. Rosenberg, S. A. Weil and I. H. Larson

Institute of Gas Technology, IIT Center,
Chicago, Illinois 60616

I. Introduction

The presence of atoms and free radicals in a methane-air flame produces not only carbon dioxide and water but also a large number of trace constituents in part-per-million and part-per-billion concentration levels. These include the oxides of nitrogen, unsaturated hydrocarbons, and partially oxygenated species. This paper will discuss the effects of flame chemistry on ethylene and the oxides of nitrogen. It will be shown that similarities do exist in the formation of these species in flames at atmospheric pressure, but the dissimilarities are of even greater interest than the similarities. In particular, ethylene is found in much higher concentrations in the flame than NO and NO₂ despite the fact that it is thermodynamically unstable whereas the nitrogen oxides are not.

Studies of the reactions of nitrogen, nitric oxide, and oxygen at high temperature indicate that the formation and disappearance of nitric oxide, the primary oxide of nitrogen found in flames and flue products, occur at very low rates.¹ With the additional fact that, in

¹ Kaufman, F. and Decker, L. J., "Seventh Symposium (International) on Combustion," Butterworths, London, 57 (1958).

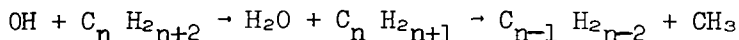
the methane-air flame and its hot reaction products, where there is usually little, if any, oxygen as such, it is apparent that the occurrence of the oxides of nitrogen are due to processes involving the reaction intermediates of the fuel-oxygen reaction. Details of such elementary processes are not known. The evidence obtained from studies on hydrogen-nitric oxide and hydrocarbon-nitric oxide flames indicates that if any nitric oxide exists in the reaction products, it is in equilibrium amounts² (that is, with nitrogen and oxygen).

² Wolfhard, H. G. and Parker, W. G., "Fifth Symposium (International) on Combustion," Reinhold, 71^a (1955).

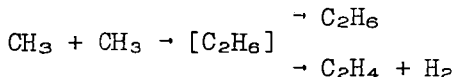
The general pattern of hydrocarbon oxidation in flames has been extensively studied although many of the detailed reactions remain to be identified and measured. It has been indicated³ that in oxygen-rich

³ Fristrom, R. M. and Westenberg, A. A., "Flame Structure," McGraw-Hill, New York, 750 (1955).

saturated hydrocarbon flames, hydrocarbons lower than the initial fuel are formed through the reaction sequence



This is the case when the initial radical formed is higher than ethyl, the CH_3 radical being split off to form the next lower olefin. In the methane-air flame, however, ethylene and other C_2 species are expected to arise as a result of the recombination of methyl radicals



From this point of view, ethylene formation in flames might be expected to follow the pattern of the cracking reaction of methane.⁴ However,

⁴ Palmer, H. B., Lahaye, J., and Hou, K. C., *J. Phys. Chem.*, **72**, 348 (1968).

it must be noted, as will be emphasized in this paper, that the rate of formation and decay of ethylene (as well as the oxides of nitrogen) cannot be considered as merely a pure pyrolysis or direct thermal reaction, the chemistry of combustion grossly interfering and competing with these mechanisms.

II. Experimental

This work was carried out with a large, single-port atmospheric pressure burner. The burner, schematically depicted in Figure 1, consists of a long vertical tube, approximately 3/4 inch in diameter, through which various methane-air mixtures are fed, surrounded by a larger annular region providing a secondary feed to the flame. By means of batch-sampling with a quartz microprobe⁵ and analysis with a

⁵ See Reference 3, Chapter 9.

Varian Aerograph series 1200 Chromatographic unit (employing a flame-ionization detector), concentration profiles for the various flat methane-air flames were obtained. A batch sampling time of about 15 seconds was used in most cases. The adjustable quartz probe was connected to the sampling and detection loop by means of Teflon-tubing. The diameter of the porous plate burner was 5.2 cm. Aeration of the primary mixture was varied from 84% to 100% to 120% of the stoichiometric air required for combustion. Primary mixture flow rates were varied from 15 to 30 SCF per hour, and secondary air flow rates were varied from 10 to 20 SCF per hour. NO and NO_2 were separated by means of molecular sieve/silica gel column. Ethylene concentration profiles were separated from other flame products by means of a column of Poropak-5 (50-80 mesh). The columns were operated at a temperature of 52°C to ensure good peak readout. Matheson Ultra-High Purity grade methane was employed in the study with no further purification.

III. Results and Discussion

A. Oxides of Nitrogen

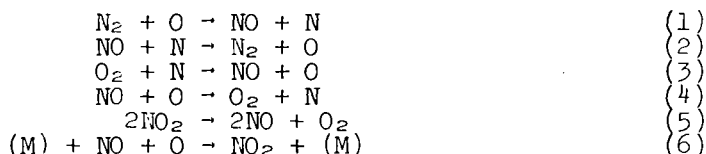
The formation of the oxides of nitrogen in methane-air flames is frequently considered as a side reaction of the combustion process; the oxides forming because air is heated to a high temperature. The data presented here indicates that this is not the case.

Figures 2 and 3 and Table 1 indicate that NO_2 is found in the "preheat" or transport region between the surface of the flat flame burner and the flame. The concentration of NO_2 increases from zero to as much as 10 ppm over this 1 mm distance. (In most cases, all reported concentrations are reproducible to within ± 1 ppm.)

The measured concentrations of the oxides of nitrogen before and after the flame show both an increase in the total, $\text{NO} + \text{NO}_2$, and a change in the ratio between these two species. For a stoichiometric methane-air flame with a secondary stream of air the concentrations are 7.5 ppm of NO_2 and 0 ppm of NO at a height of 0.1 cm. At a height of 1.1 cm (about 1.0 cm above the flame), the concentrations along the centerline of the burner have become 2.0 ppm of NO_2 and 11.0 ppm of NO . The decrease in the concentration of NO_2 is 5.5 ppm while the increase in NO is 11.0 ppm. Both Figures 1 and 2 indicate that the bulk species (nitrogen oxides) concentrations are essentially constant in the region above the flat flame.

Beyond this "flame zone" the final ratio of NO to NO_2 is strongly affected by the conditions in the "cooling" region above the flame. For example, in a stoichiometric flame the NO_2 is observed in increase from about 2 ppm at a height of 1.1 cm to almost 5 ppm at 3.6 cm above the burner. The NO concentration decreases from about 10 ppm to 7 ppm over this same distance. The total concentration remains constant at 12 ppm.

A model of the detailed chemistry of NO and NO_2 was developed to explain the rates of formation observed for the oxides of nitrogen. The reaction set includes the following reactions:



The importance of these reactions for NO_x formation in flames can be determined by comparing the calculated time required for each of these reactions to form the observed amount of NO and NO_2 with the actual time available for reaction in the flame. In this way, the relative importance of the reactions can be determined. The results are expressed for three specific regions. The regions, of course, are not independent but are closely linked to each other (Table II). The process can be visualized as follows: The fuel-air mixture leaves the burner and flows through the preheat region. Here, the gases rapidly increase in temperature because of the heat flowing back to the burner. The preheated mixture then ignites, causing a rapid change

in composition and a further increase in temperature. These rapid changes in composition from a fuel-air mixture to combustion products together with the steep temperature gradients make the flame analysis complex - hence, the segregation of the flame into regions which are easier to handle by conventional calculations.

In the preheat region, NO_2 is formed by rapid formation of NO and subsequent complete oxidation of the NO to NO_2 . The calculated residence times of reactions 1, 2, 3, and 4 are in good agreement with the actual residence time in the system. Figure 4 shows that the total concentration of the oxides of nitrogen (NO_x) increases while NO_2 decreases. The kinetics of reaction 5 adequately describe the decomposition step, while reactions 1 and 3 accounted for the increase in ($\text{NO} + \text{NO}_2$). Beyond the combustion region, the concentration of NO_x remains constant. The reaction of NO with atomic oxygen roughly predicts (within ± 10 ppm) the observed oxidation.

In an attempt to refine the calculations for the system, reactions 1 through 6 were combined with a mathematical model of a flat flame^{6,7} so that a complete time-temperature composition history of

⁶ Weil, S. A., Staats, W. R. and Rosenberg, R. B., Amer. Chem. Soc. (Div. Fuel Chem.) Preprints 10, No. 3, 84 (1966).

⁷ Weil, S. A., Institute of Gas Technology Res. Bull. No. 35, Chicago (1964).

the feed mixture could be determined. This calculation, performed on an electronic computer, did not serve to improve the disparity between observed and calculated values. The computation used the data for rate constants presently available in the literature.⁸ The combustion

⁸ Schofield, K., Planet Space Sci. 15, 643 (1967).

reactions were described by an overall kinetic expression of the form

$$\frac{d[\text{CH}_4]}{dt} = k_0 e^{-E_a/RT} [\text{CH}_4]^a [\text{O}_2]^b \quad (7)$$

The sources of the atomic species were assumed to be the equilibrium set of reactions:



The numerical predictions from this model show that this mechanism can produce only about 1 ppm of NO and almost no NO_2 . The most obvious source of error in the model is the assumption of equilibrium of O and N . It is well known that these species exist in concentrations greater than equilibrium (for N_2 and O_2 in a "non-reacting" system) but the exact concentrations at various points in an atmospheric pressure flame are not known.

B. Ethylene

The concentration of ethylene in various regions of a flame is strongly dependent upon the fuel/air ratio in the primary mixture. For a fuel-rich mixture (84% of stoichiometric air in the primary mixture with a secondary air stream), the peak ethylene concentration is almost 800 ppm. This occurs at a radial position of about 0.7 cm from the burner centerline (the burner diameter is 2.6 cm). The ethylene concentration at the centerline is about 650 ppm. For a stoichiometric primary fuel-air mixture, the maximum ethylene concentration occurs at the same point but its concentration is only 400 ppm. The concentration at the centerline of this flame is almost zero. For a fuel-lean flame (120% of stoichiometric) the maximum concentration of about 300 ppm occurs at the burner centerline. This concentration decreases slowly with distance from the center out to 2 cm. At this point, dilution by the secondary air becomes large, and the concentration decreases from about 240 ppm to about 50 ppm between 2.0 and 2.5 cm. (See Figures 5 and 6.)

One striking difference between NO_x and C_2H_4 is in the radial concentration profiles. As noted, both the fuel-rich and the stoichiometric flames show peak ethylene concentrations at 0.7 cm from the burner centerline. By contrast, the peak NO_x concentration occurs at the centerline in both of these flames, the concentration decreasing with increasing distance. The shape of the NO_x vs. distance curve changes as a function of the fuel/air ratio but the position of the maximum concentration is always at the burner centerline.

A second difference between NO_x and C_2H_4 involves the postcombustion reactions. Ethylene forms in the visible flame region in concentrations as high as 800 ppm. Most of this ethylene reacts in the post-combustion region with 3 ppm or less persisting to a height of 3.5 cm above the burner. Consequently, the conditions in the post-combustion region are of primary importance in determining the final emissions of C_2H_4 . By contrast, the total concentration of NO_x is determined by the flame and not by the post-combustion reactions. The total NO_x concentration remains constant in this region with only the ratio of NO to NO_2 changing. For example, the concentration of NO_x produced by a stoichiometric flame is about 12 ppm. Leaving the flame front, the combustion products will contain about 2 ppm of NO_2 and 10 ppm of NO. At a height of 3.5 cm, the concentrations are 5 ppm of NO_2 and 7 ppm of NO with the total concentration remaining constant.

C. Ethylene Formation in Methane-Air Flames

We have experimentally characterized the formation of ethylene (C_2H_4) in a flat methane-air flame. Analysis of the data has yielded these important conclusions:

- Oxygen has two important effects on C_2H_4 formation. 1) Oxygen or air in the primary methane-air mixture decreases the production of C_2H_4 . 2) Oxygen from the secondary air has the opposite effect. The diffusion of secondary air into the flame increases the C_2H_4 formation, with the increase being greatest for fuel-rich primary mixtures. We have developed a hypothesis for the effect of O_2 to explain this anomaly which is consistent with studies of ethylene formation in other systems.

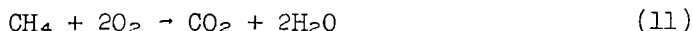
- A methane-air flame does produce significant amounts of C_2H_4 in the combustion products. As much as 5 ppm have been observed. However, almost 800 ppm of C_2H_4 is present in the visible reaction zone of the flame.
- All of the C_2H_4 forms in the visible reaction zone. Most of this C_2H_4 reacts (to form CO_2 and H_2O) downstream of the flame. Quenching the flame by impinging it on a cold surface could greatly increase the amount of C_2H_4 in the combustion products by preventing the downstream reactions of C_2H_4 .

Hypothesis for Ethylene Formation

We are postulating that ethylene forms via a reaction of some species, as yet undetermined with oxygen. This can be illustrated as follows:



The oxygen has an alternate reaction path available to it:



Thus, there is a competition for the available oxygen between species Q (which forms ethylene) and CH_4 (which does not form ethylene). It is probable that this is not the only path by which ethylene forms, another being -



The effect of oxygen in the primary methane-air mixture is to consume CH_4 . By so doing, it decreases the formation of ethylene via Reaction 12. The effect of oxygen from the secondary air is to enhance Reaction 1 and thereby increase ethylene formation.

For the fuel-rich and stoichiometric flames (Figures 5 and 6), there is a considerable difference in the C_2H_4 concentrations between the burner center line and 0.7 cm from the center line; there is more ethylene at 0.7 cm than at the center line. This must be the result of some physical or chemical difference between the two points that is caused by some outside influence on the system because temperatures and species concentrations across a flat flame burner would otherwise be uniform.

The possibility of temperature differences causing C_2H_4 concentration differences was ruled out; previously obtained profiles show that the temperature difference between these two points is only a few degrees Kelvin - not enough to account for a 150-350 ppm concentration difference.

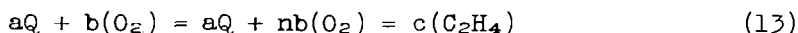
It appears that O_2 enhances the formation of C_2H_4 and that the difference in C_2H_4 concentrations between the two sampling points is the result of differing O_2 concentrations. Essentially, O_2 diffuses into the primary reaction zone from the secondary air stream. A concentration gradient results where there is approximately 0.5-3% more O_2 at a radial position of 0.7 cm than at the center line of the burner (Figures 7 and 8). The additional O_2 at 0.7 cm then causes C_2H_4 to form in excess of what is formed at the center line.

The O_2 profiles show that no oxygen from the secondary is present at the burner center line. Therefore, the value of the C_2H_4 concentration at this point is the value that would appear uniformly across the burner should no secondary air exist.

Beyond a radial position of 0.7 cm (Figures 5 and 6), the lower concentrations of ethylene are probably caused by lower temperatures overshadowing O_2 enhancement. More extensive dilution by secondary air will also account for part of the concentration decrease. In this region the formation reaction or reactions would have the potential of being speeded up by the additional O_2 found nearer the secondary. However, the lower temperatures would have the opposite effect of slowing the formation reaction. Apparently, temperature is the stronger of the two effects. This results in less C_2H_4 being produced at the edges of the burner.

The data indicate that there is also some upper limit of O_2 concentration in the primary, above which C_2H_4 formation is no longer detectably enhanced by secondary O_2 . For a 120% of stoichiometric flame composition, where considerable excess O_2 already exists in the primary reaction zone, the highest C_2H_4 concentration is at the center line and steadily decreases away from the center line (Figure 9).

We believe the excess O_2 from the primary stream overshadows any effect of O_2 from the secondary stream. For example, if some species Q reacts with O_2 to form C_2H_4 and the reaction is fast enough so that all of Q reacted prior to sampling, then the addition of even more O_2 (from the secondary) would not result in detecting more C_2H_4 :



where $n > 1$.

Literature lends support to the postulate of O_2 enhancing ethylene formation. Some related experiments by Robertson and Matson (reported by Minkoff and Tipper⁹) indicate that the addition of small quantities

⁹ Minkoff, G. J. and Tipper, C.F.H., "Chemistry of Combustion Reactions," London, Butterworths (1962).

of O_2 - up to 2% - to a fuel-rich acetylene mixture can increase ethylene production. More recently, Fenimore and Jones,² investigating ethylene flames, found the same indications of O_2 enhancement. The work of Haskell¹⁰ on the pyrolysis of propane between 350° and 700°C

¹⁰ Haskell, W. W., Dissert. Abst. 18, 80 (1958).

shows that an increase in ethylene formation is caused by the addition of small amounts of O_2 . The applicability of Haskell's work to the combustion of CH_4 is, however, in doubt.

Ethylene in Combustion Products

Our subsequent studies of ethylene formation will center around the primary reaction region because little or no formation occurs in other regions of this specific flame. The C_2H_4 concentration drops drastically just beyond the reaction zone and then remains essentially constant. The drop in concentration is approximately 500 ppm (Figure 1) and is probably due to the reaction of CH_4 with O_2 to form CO_2 and H_2O . The result is a final concentration of 0.5 to 3 ppm just beyond the reaction zone. The flue gas exiting from the experimental chamber also contains about 3.0 ppm of C_2H_4 . This concentration can presumably be enhanced if the C_2H_4 reactions are prevented from occurring, such as by quenching.

IV. Conclusion

The data of this work have confirmed that the formation of the oxides of nitrogen in atmospheric methane-air flames is primarily determined by the combustion chemistry with the chemistry of heated air playing a secondary role. Two different processes describe the NO_x -methane flame system: a) the decomposition of NO_2 to NO , and b) formation of additional NO from N_2 and O_2 -derived flame species. The disparity between calculated and observed values is attributed to the lack of a quantitative inclusion of the effects of "superequilibrium" concentrations of N and O atoms.

Ethylene is shown to form to a very large extent within the combustion zone of the flame (visible region). Although the final flue products contain little ethylene, concentrations approaching one part per thousand or observed in this flame region. Ethylene formation in flames is seen to be dependent upon post-combustion reactions whereas NO and NO_2 formation depend only upon flame zone reactions.

V. Acknowledgement

The authors wish to express their grateful appreciation to the American Gas Association whose support made this work possible.

Table I. CONCENTRATION CHANGES OF NO AND NO₂ WITH INCREASING HEIGHT OF THE BURNER FOR A STOICHIOMETRIC METHANE-AIR FLAME WITH AN AIR SECONDARY

	<u>0.0</u>	<u>-0.7</u>	<u>1.4</u>
	ppm		
0.1 cm Above Burner			
NO	0.0	0.0	0.0
NO ₂	7.5	7.1	5.7
NO + NO ₂	7.5	7.1	5.7
1.1 cm Above Burner			
NO	11.0	2.0	0.0
NO ₂	2.0	5.6	3.5
NO + NO ₂	13.0	7.6	3.5
Conc. Increases			
NO	+11.0	+2.0	0.0
NO ₂	-5.5	-1.5	-2.2
NO + NO ₂	+5.5	+0.5	-2.2

Table II. CALCULATED AND ACTUAL RESIDENCE TIMES*

	<u>Calculated</u>	<u>Actual</u> Seconds	<u>Difference</u> [†]
<u>In the Preheat Region</u>			
$N_2 + O \rightarrow NO + N$	0.587×10^{-2}	1.22×10^{-2}	-0.634×10^{-2}
$O_2 + N \rightarrow NO + O$			
$N_2 + O_2 \rightarrow 2NO$	2.0×10^1	1.22×10^{-2}	$\approx 2.0 \times 10^1$
$NO + O \rightarrow NO_2$	2.12×10^{-2}	1.22×10^{-2}	$+0.90 \times 10^{-2}$
$2NO + O_2 \rightarrow 2NO_2$	4.25×10^{15}	1.22×10^{-2}	$\approx 4.25 \times 10^{15}$
<u>In the Combustion Region</u>			
$N_2 + O \rightarrow NO + N$	0.35×10^{-2}	1.04×10^{-1}	-0.965×10^{-1}
$O_2 + N \rightarrow NO + O$			
$2NO_2 \rightarrow 2NO + O_2$	0.78×10^{-2}	1.04×10^{-1}	-0.922×10^{-1}
$N_2 + O_2 \rightarrow 2NO$	1.1×10^1	1.04×10^{-1}	$\approx 1.1 \times 10^1$
<u>In the Cooling Region</u>			
$NO + O \rightarrow NO_2$	5.0×10^{-2}	6.25×10^{-2}	-1.25×10^{-2}
$2NO + O_2 \rightarrow 2NO_2$	4.8×10^{15}	6.25×10^{-2}	$\approx 4.8 \times 10^{15}$

* The comparison of these reactions has been made on the basis of the residence time of reaction necessary to form the experimental observed quantity of NO_x .

† Seconds calculated minus seconds actual.

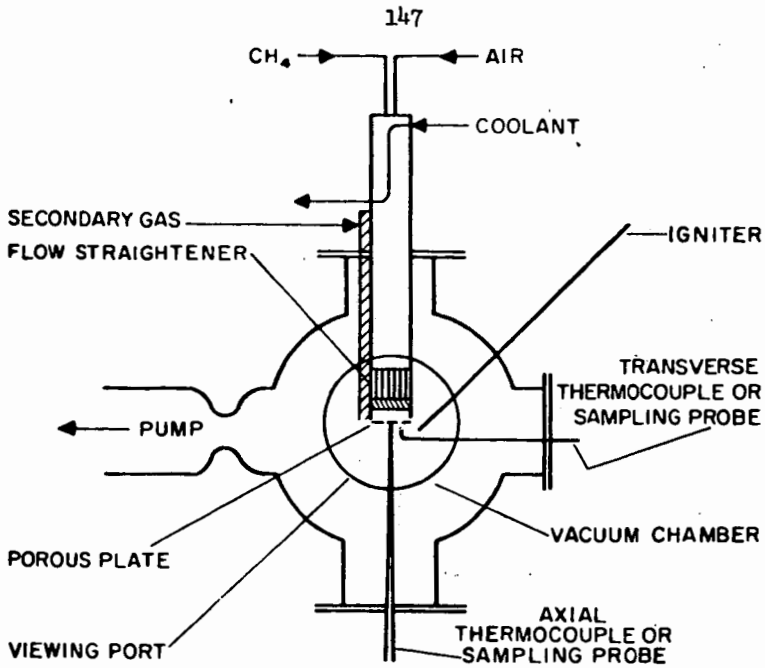


Fig. 1. - BURNER DESIGNED TO DETERMINE CHEMISTRY OF NITROGEN OXIDES PRODUCED IN METHANE-AIR FLAMES

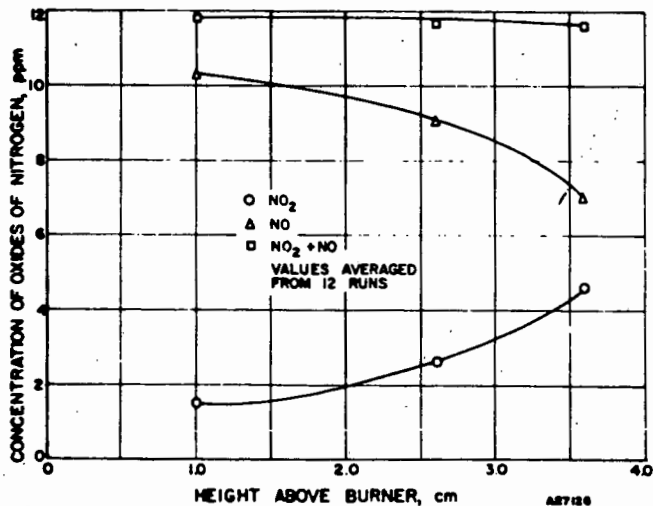


Figure 2. TOTAL CONCENTRATION OF OXIDES OF NITROGEN IN A METHANE-AIR STOICHIOMETRIC FLAME AT THE BURNER CENTER LINE

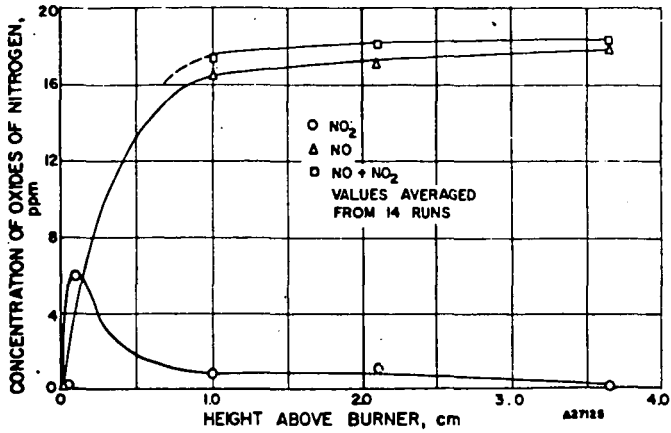


Figure 3. TOTAL CONCENTRATION OF OXIDES OF NITROGEN IN A FUEL-RICH (84% of Stoichiometric) FLAME AT BURNER CENTER LINE

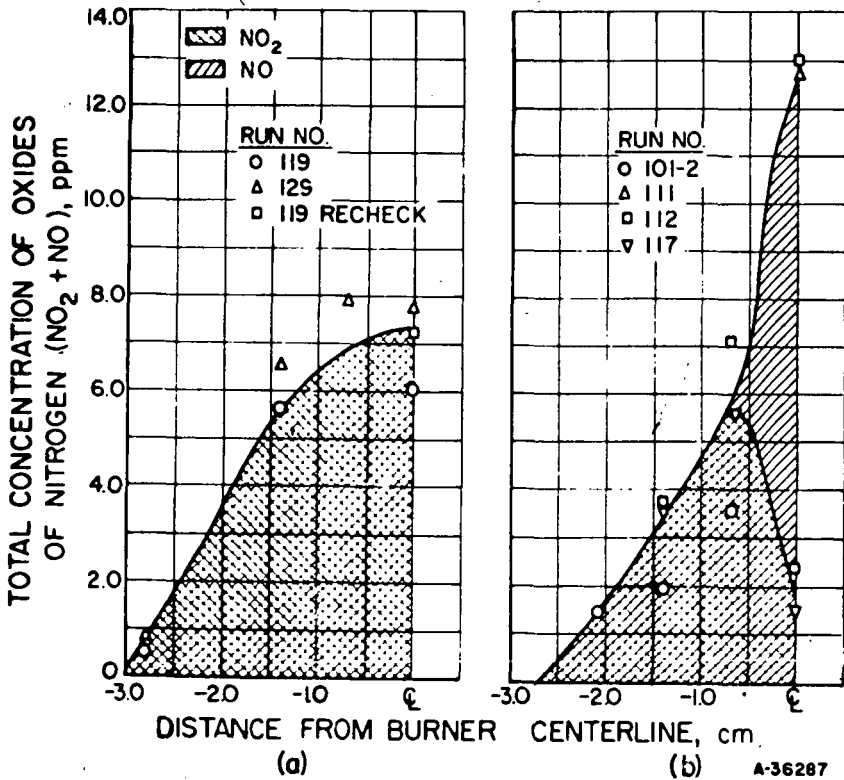
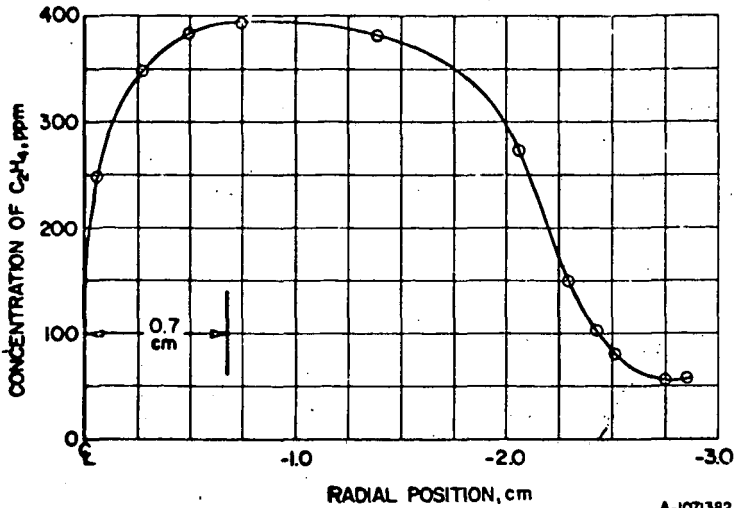
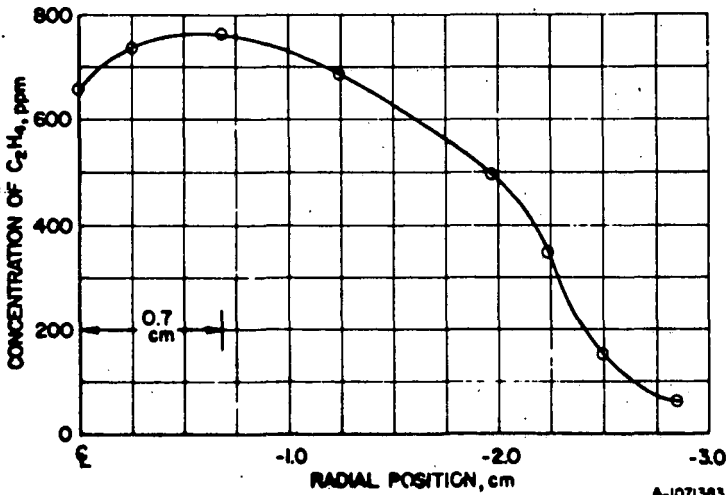


Figure 4. TOTAL CONCENTRATION OF NITROGEN FOR A METHANE-AIR STOICHIOMETRIC FLAME AT a) 0.1 cm AND b) 1.1 cm ABOVE BURNER



A-1071382

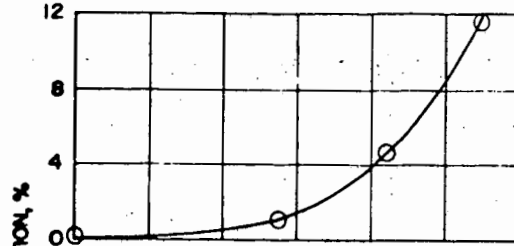
Figure 5. ETHYLENE CONCENTRATION AS A FUNCTION OF RADIAL POSITION AT 0.1 cm ABOVE THE BURNER FOR STOICHIOMETRIC CH_4 -AIR FLAME



A-1071383

Figure 6. ETHYLENE CONCENTRATION AS A FUNCTION OF RADIAL POSITION AT 0.1 cm ABOVE THE BURNER FOR 84% OF STOICHIOMETRIC CH_4 -AIR FLAME

(a)



(b)

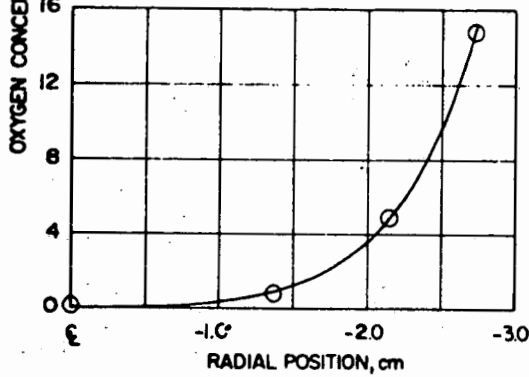
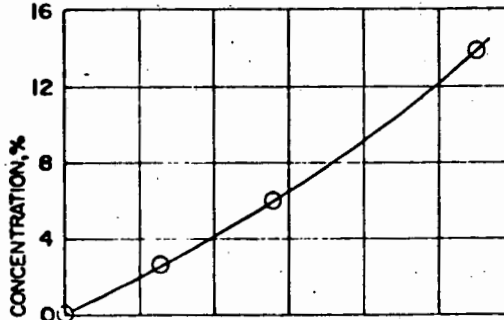


Figure 7. OXYGEN CONCENTRATION IN 84% OF STOICHIOMETRIC CH₄-AIR FLAME (From Secondary Air Only) AT a) 1.1 cm AND b) 0.5 cm ABOVE BURNER

(a)



(b)

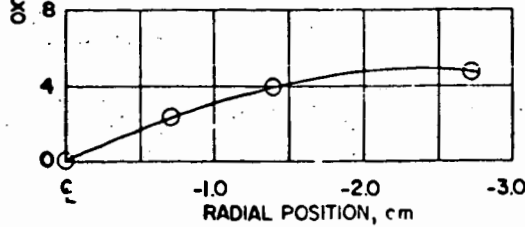


Figure 8. OXYGEN CONCENTRATION IN 100% OF STOICHIOMETRIC CH₄-AIR FLAME (From Secondary Air Only) AT a) 1.1 cm AND b) 0.5 cm ABOVE BURNER

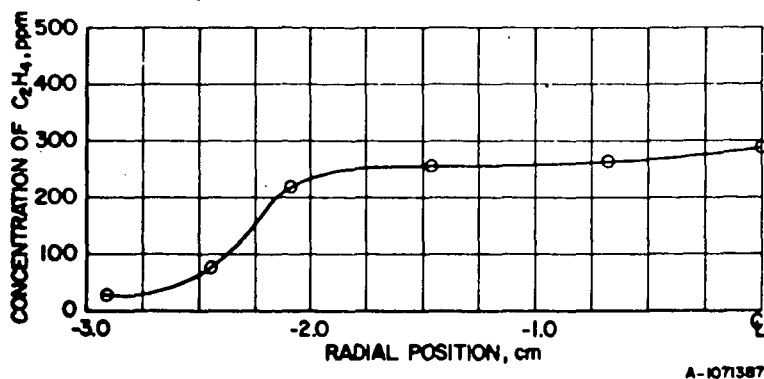


Figure 9. ETHYLENE CONCENTRATION AS A FUNCTION OF RADIAL POSITION AT 0.1 cm ABOVE BURNER FOR 120% OF STOICHIOMETRIC CH₄-AIR FLAME

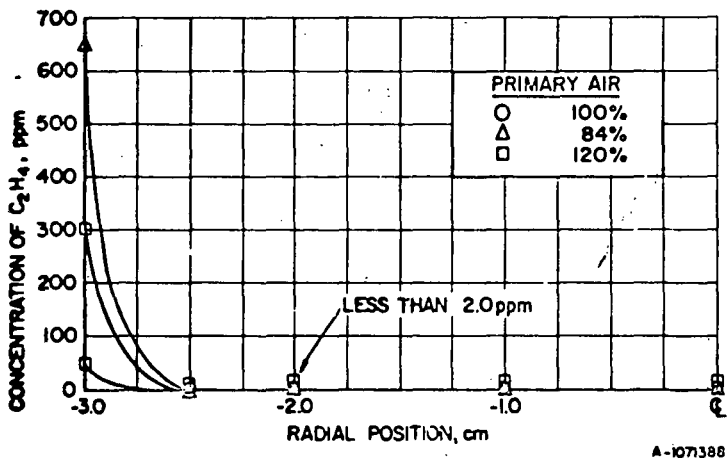


Figure 10. CONCENTRATION OF ETHYLENE AT CENTER LINE OF CH₄-AIR FLAMES

Fast-Flow Kinetic Studies of Methane Reactions with Atomic Oxygen at Room Temperature

R. V. Serauskas and R. A. Keller

Institute of Gas Technology, IIT Center
Chicago, Illinois

I. Introduction

Many contributions to kinetic rate knowledge have resulted from premixed flame studies.^{1,2,3} A flame, consisting of a multi-reaction complex medium, lends

1. R. M. Fristrom, and A. A. Westenberg, "Flame Structure," McGraw-Hill, New York (1965).
 2. S. W. Benson, "The Foundations of Chemical Kinetics," McGraw-Hill, New York, 276 (1960).
 3. N. Basco and R.G.W. Norrish, *Can. J. Chem.* **38**, 1769 (1960).
- itself to unambiguous kinetic analysis only with difficulty. Specifically, the more recent flame studies of combustible methane mixtures⁴ have directed much inter-
4. R. M. Fristrom, C. Grunfelder, and S. Favin, *J. Phys. Chem.* **64**, 1386 and 1393 (1960).

est of late toward the elementary reactions in the methane oxidation scheme. New and improved techniques for the study of atom and radical reactions have led to renewed kinetic studies which have confirmed some earlier results and have been at odds with others. The addition of various chemically perturbing agents to the O-atom/CH₄ system, for example, allow for the study of some elementary oxidation reactions at room temperature by the more convenient and unambiguous flow-discharge techniques. However the results in all cases have not been uniform, especially in systems containing oxygen.⁵

5. F. Kaufman, in "Progress in Reaction Kinetics," Vol. 1 (ed. G. Porter), Pergamon Press, New York, 1 (1961).

In this work, a number of methane-oxygen reactions have been studied employing a fast-flow reaction system, coupled directly with a Bendix model 3015 time-of-flight mass spectrometer. N and H-atom titrations as well as Woods-Bonhoeffer discharges are employed in generating the active species.

II. Experimental

The reaction system employed is depicted schematically in Figure 1. A Woods-Bonhoeffer discharge-flow system is in train with a Bendix model 3015 time-of-flight mass spectrometer. Atoms or radicals enter in the central annular space in the reaction train. Reactants enter through the central tube fitted with a Teflon "Swage" gland to permit movement along the reaction train axis. In this way, the distance of the mixing region from the molecular leak (aluminum foil disk with an 0.005 inch pinhole) can be varied. A 40 liter/sec Stokes' pump throttled through a linear flow velocity of about 10 meters/sec and a reaction region pressure in the 10 to 1000 millitorr range. Knowing the volumetric flow rate, v , and the diameter, d , of the reactor, the distance, z , of the tube mouth from the TÖF sampling leak can be related to the time variable, t , in an absolute fashion by the relation:

$$t = \left(\frac{\pi d^2}{4v}\right) z^{-1}$$

This reaction holds strictly for the case of a cylindrical reactor and laminar flow.⁵ The methane, used without further purification, was Matheson Ultra-High Purity grade. Matheson Research grade HCl was employed in the catalytic study. Matheson High Purity grade NO₂ was redistilled in vacuo for use in the generation of OH radicals. The oxygen used was Ultra-High Purity grade Matheson, employed without further purification.

Oxygen atoms were generated by two methods: (1) the discharge of a 1 to 9 O₂/Ar mixture (2) the very rapid gas-phase titration of NO by N atoms (N + NO →

N_2+O), the N atoms being generated by discharging N_2 . The hydroxyl radicals were generated by the rapid gas phase titration of NO_2 with H atoms ($H+NO_2 \rightarrow NO+OH$), the H atoms being generated by discharge of a 5% $H_2/95\%$ Ar mixture containing a trace of water in order to aid dissociation (The walls of the reaction train were coated with phosphoric acid to give low, reproducible wall-recombination effects.) In all cases the temperature remained within 1° of $298^\circ K$.

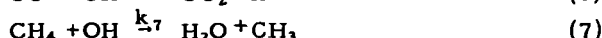
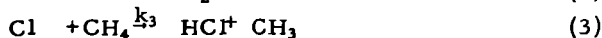
III. Results and Discussion

A. Methane-O-atom Reaction with HCl Catalyst

At room temperature the reaction between methane and atomic oxygen is extremely slow because the reaction has a heat of activation between 8-9 kcal/g-mole.¹ Consequently, if one wished to study the reaction, the investigation must be conducted at elevated temperatures or a suitable catalyst must be added for room temperature studies.

We selected hydrogen chloride gas as a catalyst for this study because it is known to accelerate the reaction between methane and atomic nitrogen.

The following reactions may be considered in this system:



This reaction scheme yields a series of 12 simultaneous differential equations that are extremely difficult to solve analytically.

As a first approximation, we might eliminate all of the reactions with an energy of activation of 8 kcal/g-mole or more. At $300^\circ K$, the difference in rate between a reaction with $E_a = 4$ kcal/g-mole and one with 8 kcal/g-mole is a factor of about 10^3 . Thus, two reactions with approximately equal reactant concentrations and frequency factors will differ in rate by 1000 if they have such an activation energy difference.

Using this criterion, Table I^{1,6} shows that Reaction 7 through 11 can be eliminated from the reaction scheme. K. Schofield, *Planet. Space Sci.* 15, 643 (1967).

We will show later that an error has apparently been introduced by eliminating Reaction 9. The concentration of H atoms apparently is sufficiently high to offset the activation energy difference.

A second approximation involves the "steady-state assumption." This assumption specifies that the rate expressions for all of the active species be set equal to zero. For example, the rate of formation of chlorine atoms is as follows:

$$\frac{d(Cl)}{dt} = k_1(HCl)(O) - k_3(Cl)(CH_4) \quad (13)$$

Using the steady-state assumption yields the following equation:

$$k_1(HCl)(O) - k_3(Cl)(CH_4) = 0 \quad (14)$$

The following equations are obtained by using the steady-state assumption for CH_2 , CH_3 , and OH :

$$k_4(\text{CH}_3)(\text{O}) - k_5(\text{CH}_2)(\text{O}) = 0 \quad (15)$$

$$k_3(\text{Cl})(\text{CH}_4) - k_4(\text{CH}_3)(\text{O}) = 0 \quad (16)$$

$$k_1(\text{HCl})(\text{O}) - k_2(\text{OH})(\text{O}) + k_4(\text{CH}_3)(\text{O}) - k_6(\text{CO})(\text{OH}) = 0 \quad (17)$$

This series of four algebraic equations can now be solved for the concentrations of the active species:

$$(\text{Cl}) = \frac{k_1(\text{HCl})(\text{O})}{k_3(\text{CH}_4)} \quad (18)$$

$$(\text{CH}_2) = \frac{k_1(\text{HCl})}{k_5} \quad (19)$$

$$(\text{CH}_3) = \frac{k_1(\text{HCl})}{k_4} \quad (20)$$

$$(\text{OH}) = \frac{2k_1(\text{HCl})(\text{O})}{k_2(\text{O}) + k_6(\text{CO})} \quad (21)$$

The rates of the reactions of O, CO, and CO₂ can now be written and simplified using the above expressions for the concentrations of the active species.

$$\frac{d(\text{O})}{dt} = -3k_1(\text{HCl})(\text{O}) - \frac{2k_1k_2(\text{HCl})(\text{O})^2}{k_2(\text{O}) + k_6(\text{CO})} \quad (22)$$

$$\frac{d(\text{CO})}{dt} = k_1(\text{O})(\text{HCl}) - \frac{2k_1k_6(\text{HCl})(\text{O})(\text{CO})}{k_2(\text{O}) + k_6(\text{CO})} \quad (23)$$

$$\frac{d(\text{CO}_2)}{dt} = \frac{2k_1k_6(\text{HCl})(\text{O})(\text{CO})}{k_2(\text{O}) + k_6(\text{CO})} \quad (24)$$

For the conditions of this study, $(\text{CO}) < 1/5 (\text{O})$ so that $k_2(\text{O}) \gg k_6(\text{CO})$. The rate expression for the disappearance of atomic oxygen is, therefore:

$$+ \frac{d(\text{O})}{dt} = -5k_1(\text{HCl})(\text{O}) \quad (25)$$

Integrating this expression yields -

$$\ln(\text{O}) = -5k_1(\text{HCl})t + \ln(\text{O})_0 \quad (26)$$

With $t = \text{time} = \frac{z}{u}$, $z = \text{reactor distance}$, and $u = \text{linear flow velocity}$,

$$\ln(\text{O}) = -5k_1(\text{HCl})\frac{z}{u} + \ln(\text{O})_0 \quad (27)$$

Therefore, a plot of $\ln(\text{O})$ vs. z should yield a straight line. Figure 2 shows the experimental data plotted in this manner. The reaction exhibits first-order behavior between 100 and 300 mm, but deviates from this behavior beyond this point. It almost appears that the reaction stops shortly beyond the 300-mm point. Our analysis will concentrate on the first 300 mm of the reactor. In this region the slope of the curve yields a rate constant of 2.65×10^{-15} cu cm/particle-sec. If this reaction has a steric factor of 0.1, the activation energy is about 5 kcal/g-mole.

This value for the rate constant is consistent with the postulated mechanism. The rate expression for O atom disappearance (Equation 25) shows that Reaction 1 is the slowest or rate-controlling step of the mechanism. Comparison of the value of $k_1(2.65 \times 10^{-15})$ with the values in Table II shows that this is indeed the case.

Equation 23 for the formation of CO can be simplified by applying the values of the rate constants and the various concentrations:

$$\frac{d(\text{CO})}{dt} = k_1(\text{O})(\text{HCl}) \quad (28)$$

Substituting the expression for the O atom concentration yields -

$$\frac{d(\text{CO})}{dt} = k_1(\text{HCl})(\text{O})_0 e^{-5k_1(\text{HCl})t} \quad (29)$$

Integrating Equation (29) yields -

$$(\text{CO}) = \frac{(\text{O})_0}{5} [1 - e^{-5k_1(\text{HCl})\frac{z}{u}}] \quad (30)$$

The rate expression for CO₂ can now also be integrated:

$$(\text{CO}_2) = \frac{0.4k_1k_6}{k_2} (\text{HCl})(\text{O})_0 \left[t + \frac{e^{-5k_1(\text{HCl})t} - 1}{5k_1(\text{HCl})} \right] \quad (31)$$

The integrated expressions show the correct qualitative details for the reaction, but the quantitative predictions are not accurate. For example, the equations

predict that CO should be present in greater concentrations than CO₂. Figure 3 shows that this effect is indeed observed. However, the quantitative predictions are not in agreement; the predicted rates of formation are too low.

Another qualitative feature of the reaction is shown in Figure 4. The amount of CO formed increases by a factor of 5 (in the early stages of the reaction) as the initial HCl concentration is increased. This is predicted by Equation (30).

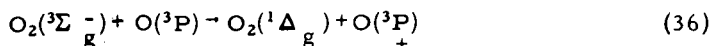
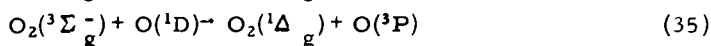
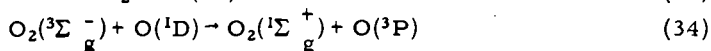
The equations predict the qualitative but not the quantitative features of the experimental data. The data quality has been determined from a mass balance on the reactants and products. About 80% of the O atoms that react are recovered as either CO or CO₂. The reaction also forms water and molecular oxygen. The amount of water is quite small and the amount of O₂ formed is also small and cannot be accurately determined because of the large background O₂ concentration. Within these limitations, the mass balance is good and indicates that the data are internally consistent. From this, it appears that the reaction scheme is incomplete.

The most probable discrepancy in the proposed scheme is the elimination of Reaction (9). This reaction can be rapid if the concentration of H atoms is sufficiently high. H atoms are formed by Reactions (2) (a very fast reaction), (5), and (6). Therefore, they may be present in a sufficiently high concentration to make Reaction (9) significant. Reaction (9) produces both CH₃ and OH radicals. CH₃ reacts, via CH₂, to form CO, and the CO is oxidized to CO₂ by OH. Hence, inclusion of Reaction (9) should provide for faster rates of CO and CO₂ formation.

B. Possible Influence of Excited O₂

The above data shows that about 25% of the original methane will be converted to products (CO + CO₂) over a reaction zone length of 350 mm. Figure 5 presents some data for this system, comparing the reaction of discharged O₂ with CH₄ to that of O atoms generated in the titration of NO with N atoms. Curve A indicates the formation of CO₂ from a CH₄/HCl mixture using O atoms generated in the gas-phase titration: N + NO → N₂ + O. Curve B gives the data for the same system after adding about 15 X 10⁻³ mm Hg of ground-state O₂ to the atom stream, which also contains about 15 X 10⁻³ mm Hg of O atoms as determined by the gas-phase titration. Discharged O₂ (with about 15 X 10⁻³ mm Hg of O atoms and 15 X 10⁻³ mm of Hg of O₂) used in place of the O atom stream obtained by titration yields Curve C, which shows considerable enhancement of the combustion process over Curves A and B. The data of Curves A and B lend support to the possibility of a specific effect of molecular oxygen on O atom reactions; excited-state molecular O₂ may be the chemically perturbing agent for these systems.

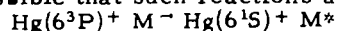
The only difference between Curves C and B is that the former presents data for the CH₄/HCl/O system in the presence of excited molecular O₂, while the latter involves only added ground-state O₂. In an electrical discharge, the following processes can take place:



The radiative loss rate constant for O₂(¹Σ⁺) may be as large as 10⁻¹³cc/particle-sec. and 10⁻²²cc/particle-sec. for O₂(¹Δ_g),⁸ thus allowing O₂(¹Δ_g) to interfere in chemical reaction systems at moderate ⁸ to rapid flow rates.⁷ ⁸ (Although quite

7. A. M. Falick and B. H. Mahan, *J. Chem. Phys.* 47, 4778 (1967).
inert toward saturated hydrocarbons, O₂(¹Δ_g) is known to react readily with atoms, free-radicals, and unsaturated compounds.)⁸

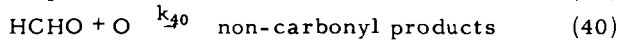
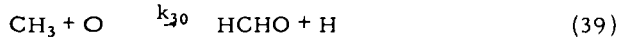
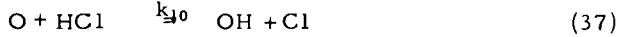
It is also possible that such reactions as



may occur in systems manometered with mercury, this effect should be observable regardless of the type of discharge used. Preliminary indications show that (37) is not significant in our system.

C. Detection of Carbonyls in CH₄-O atom Reactions

Our flow system provides for a "residence time-to-reaction length" ratio of $t/z = u^{-1} \approx 1$ msec/cm. (The linear flow rate is about 10 meters/sec.) The kinetic data points are usually spaced 10 cm apart. Therefore, any formaldehyde originally formed in the reaction of methyl radicals with O atoms must be reduced to a concentration lower than the detectable limit (about 1.60×10^{13} molecules/cu cm in this case) within 0.01 sec. The problem of HCHO formation can then be demonstrated by a crude estimate employing the following simplified steady-state scheme:



$$\frac{d[\text{Cl}]}{dt} = \frac{d[\text{CH}_3]}{dt} = \frac{d[\text{HCHO}]}{dt} = 0 \quad (41)$$

Then,

$$[\text{Cl}] = \frac{k'_{10}[\text{O}][\text{HCl}]}{k_{20}[\text{CH}_4]} \quad (42)$$

$$[\text{CH}_3] = \frac{k_{20}[\text{CH}_4][\text{Cl}]}{k_{30}[\text{O}]} \quad (43)$$

$$[\text{HCHO}] = \frac{k_{30}[\text{O}][\text{CH}_3]}{k_{40}[\text{O}]} = \frac{k_{30}}{k_{40}}[\text{CH}_3] \quad (44)$$

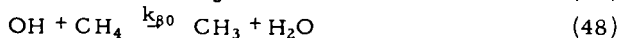
Thus,

$$[\text{HCHO}] = \frac{k'_{10}}{k_{40}}[\text{HCl}] \quad (45)$$

With $[\text{HCHO}] = 0.5$ millitorr and $[\text{HCl}] = 20$ millitorr, and with an estimated $k'_{10} \approx 10^{-12}$ cu cm/mole-sec, the most reliable data for Reaction 40 yields a value $k_{40} \approx 8 \times 10^{-13}$ cu cm/mole-sec, which would make the steady-state value of $[\text{HCHO}] \approx 25$ millitorr, an amount readily detectable by the 3015 TOF. In short, if carbonyls are intermediates in the reaction of CH₄ with O atoms at room temperature, our results demand that they be present as reactive species (such as formyl radicals, HCO) rather than stable molecules.

D. Reaction of OH with CH₄

The primary scheme associated of OH radicals in the flow reactor is as follows:



(The initial reaction to produce OH has $k_5 \gg k_6, k_7,$ and $k_8,$ and hence the conversion of H into OH is considered to be instantaneous.) In the absence of methane, the k_8 step is noncontributing and -

$$\text{Rate}(\text{OH}) = + \frac{d[\text{OH}]}{dt} = -k_{60}[\text{OH}]^2 - k_{70}[\text{O}][\text{OH}] - \gamma_{\text{OH}}[\text{OH}] \quad (50)$$

Since k_{60} and k_{70} are comparable at room temperature, we may assume a steady-state condition for O atoms such that $d[\text{O}]/dt = 0$. This yields $k_{70}[\text{O}] = k_{60}[\text{OH}]$ and hence,

$$\text{Rate}(\text{OH}) = \frac{d[\text{OH}]}{dt} = -2k_{60}[\text{OH}]^2 - \gamma_{\text{OH}}[\text{OH}] \quad (51)$$

In the presence of CH_4 , k_{80} contributes and, assuming that CH_4 does not alter the kinetic wall behavior of OH ,

$$\text{Rate}_{(\text{CH}_4, \text{OH})} = \frac{d[\text{OH}]}{dt(\text{with CH}_4)} = -2k_{60}[\text{OH}]^2 - (k_{80}[\text{CH}_4] + \gamma_{\text{OH}})[\text{OH}] \quad (52)$$

Both Equations 17 and 18 are of the form -

$$\frac{dy}{dt} = -y(ay + b) \quad (53)$$

(with $y = [\text{OH}]$) which may be solved by the substitution -

$$\mu = \frac{y}{ay + b} \quad (54)$$

which yields

$$\frac{\mu}{\mu_0} = e^{-bt} \quad (55)$$

$[\text{CH}_4]$ is assumed essentially constant since its concentration is 59 times greater than $[\text{OH}]$ in this system.

Figure 6 presents some recent data on the fast-flow reaction between CH_4 and OH . (\square indicates the reaction without CH_4 ; \circ indicates the reaction in the presence of CH_4 .)

In this system, $k_{80} \ll 2k_{60}$ and $(k_{80}[\text{CH}_4] + \gamma) \ll 2k_{60}[\text{OH}]$. These numerical values make it difficult to use the method of initial rates to analyze the data. However, it is possible to use the integrated rate equation (55). This equation can be simplified by expanding the exponential term, e^{-bt} , as a power series, neglecting the higher powers of bt since they are much less than unity:

$$\frac{y_0/(y_0 + b)}{y/(ay + b)} \approx 1 + \left(\frac{b}{vz}\right) z = 1 + bt \quad (56)$$

or rearranging Equation (56) yields -

$$y^{-1} \approx \left[\frac{1}{vz} (a + by_0^{-1}) \right] z + y_0^{-1} \quad (57)$$

Thus, a plot of y^{-1} against z (reciprocal of $[\text{OH}]$ versus distance, z , from inlet) should be linear. From the difference in slopes of two such straight lines (one for a run with CH_4 , one for a run without it) one can obtain k_4 , the rate constant in question. The data plotted in Figure 7 show the predicted linear relation.

From Equation 57, the definitions of a , b , and y , and setting $\text{SLOPE}_{\text{CH}_4}$ and SLOPE_0 equal to the slopes of the y^{-1} versus z curves for the run with CH_4 and the run without, respectively, yields -

$$k_{80}[\text{CH}_4] = [\text{OH}]_0(\text{CH}_4) [v_{\text{CH}_4} (\text{SLOPE}_{\text{CH}_4}) - 2k_{60}] - [\text{OH}]_0(\text{O}) [v_0(\text{SLOPE}_0) - 2k_{60}] \quad (58)$$

From Figure 10 and the 3015 sensitivity value for OH (1.60×10^{13} particles/cu cm = 10 units), and using the reported value⁶ for k_{60} (2.5×10^{-12} cu cm/part-sec) we have -

$$2k_{60} = 80 \text{ unit}^{-1} \text{ sec}^{-1}$$

$$[\text{OH}]_b(\text{CH}_4) = 10 \text{ units}$$

$$[\text{OH}]_b(\text{O}) = 7.0 \text{ units}$$

$$\text{SLOPE}_{\text{CH}_4} = 0.0326 \text{ unit}^{-1} \text{ cm}^{-1}$$

$$\text{SLOPE}_0 = 0.0474 \text{ unit}^{-1} \text{ cm}^{-1}$$

In the run with CH_4 , the flow rate $v_{\text{CH}_4} = 2.635 \times 10^3 \text{ cm-sec}^{-1}$. Thus, $k_{80}[\text{CH}_4] = 58.94 \text{ sec}^{-1}$. Since $[\text{CH}_4] = 2.43 \times 10^{16} \text{ molecules/cu cm}$, we have $k_{80} = 2.42 \times 10^{-15} \text{ cu cm/particle-sec}$. This is roughly an order of magnitude lower than that recently reported by Greiner,⁸ and about 3 times lower than that reported by Wilson

8. N. R. Greiner, J. Chem. Phys. 46, 490 (1967).

and Westenberg.⁹ In the absence of data at other temperatures we may use the
 9. W. E. Wilson and A. A. Westenberg, "11th Symposium (International) on Com-
 bustion," Combustion Institute (1967).

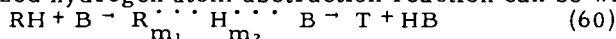
approximate collision theory argument² that the rate constant is given by -

$$k_{30} = 10^{-10} \cdot 5 e^{-E_a/RT} \quad (59)$$

which gives an activation energy of 5.65 kcal/mole for the $\text{CH}_4 + \text{OH}$ reaction.

Whether at high or low temperatures, a chain propagation step in the combustion process for a hydrocarbon is the abstraction of a hydrogen atom from the hydrocarbon by atomic oxygen or hydroxyl.

The generalized hydrogen atom abstraction reaction can be written¹⁰



10. H. S. Johnston, "Gas Phase Reaction Rate Theory," Ronald Press, New York (1966).

where m_1 and m_2 are the bond orders, in the transition state, of the "breaking bond" $\text{R} \cdot \cdot \cdot \text{H}$ and the "forming bond" $\text{H} \cdot \cdot \cdot \text{B}$. This bond-order concept has its intuitive appeal to the chemist and structural chemist on the bases of bond length, bond strength, and coordinating valence. Thus, in a single covalent bond involving one pair of shared electrons as in H_2 or HCl , the bond order is 1. In nitrogen, however, since one may see that there are three pairs contributing to bonding (a so-called " $\sigma_{2p} \pi_{4p}$ " configuration) the bond order there is 3. The important result here is to remember that, in the bimolecular reaction above, the underlying assumption is that the sum of bond orders remains constant throughout such abstraction reactions. That is, $m_1 + m_2 = 2$.

One may then treat such reactions by assuming a valence bond potential for the transition state given by

$$V = D_{\text{RH}} - C_{\text{RH}}(m_1^p) - D_{\text{HB}}(m_2^q) + V_r \quad (61)$$

where the D's are the bond dissociation energies, V_r is the energy of repulsion arising from the parallel electron spins on R and B, and q are empirical parameters indicating the strength of the intermolecular valence forces. For oxygen species where triplet states are involved (two parallel electron spins on the same species), twice the repulsion energy has to be included for a more reasonable estimate.

Recently, our results indicated a room temperature rate constant of about 10^9 cu cm-mole⁻¹-s⁻¹ for the $\text{OH} + \text{CH}_4 \rightarrow \text{CH}_3 + \text{H}_2\text{O}$ reaction. This implies that the activation energy for such a reaction is about 5 to 6 kcal-mole⁻¹. The bond energy-bond order method yields about 5 kcal-mole⁻¹ as an activation energy.

We have also indicated that the combustion of methane is significantly enhanced in the presence of discharged rather than titrated oxygen. Our first interpretations associated this extra activity with excited O_2 , namely (Δ g) O_2 . Table III is a brief compendium of rate constants and activation energies as calculated by the bond energy-bond order method.

From the above table, it is obvious that the $\text{CH}_4 + \text{O}_2(\Delta\text{g})$ reaction should be about 10,000 times more rapid than the ground-state O_2 reaction at flame temperatures. Although the Σg^+ state of O_2 indicates an even greater reaction, the lifetimes (collisional and radiative) for this species are much too short to complete with that for the Δg state (46 minutes). Thus, no significant concentration of this Σg^+ species is expected. Each of the rate constants¹¹ in Table III is computed by the prescription

11. S. W. Mayer and L. Schieler, J. Phys. Chem. 72, 2628 (1968).
 of activated complex theory. Successive variation of the parameters of Equation 8 leads to a "saddle point curve," or curve of steepest ascent. The maximum of this path may be taken as the activation energy, E_a . Assuming a linear complex, one can readily calculate the rate constant from

$$k_{\text{rate}} = K \frac{kT}{h} \cdot \frac{Q^\ddagger}{Q_A Q_B} e^{-E_a/RT} \quad (62)$$

where the Q_A and Q_B are reactant partition functions, Q^\ddagger is the partition function of the complex, R is the gas constant (in cal-mole⁻¹-deg⁻¹ if E_a is in cal-mole⁻¹), k is Boltzmann's constant, h is Planck's constant, and K is the transmission coefficient

for the potential barrier. Quantum mechanically, even though the energy of a system is less than the potential at that point, there is a finite probability of finding the system in the configuration beyond that point. This probability is the transmission coefficient, and the "process" is referred to as quantum-mechanical "tunnelling." In any event, Equation 62 can be readily calculated for most simple reactions and has been shown to give very reliable estimates of the rate constants for a great number of elementary reactions.

It should be observed that the reactions in Table III for $\text{CH}_4 + \text{O}_2$ are not as fast as the corresponding reactions with O atoms. However, one would expect that the reactions of $\text{O}_2(^1\Delta_g)$ with CH_3^\cdot radicals or with unsaturated hydrocarbon intermediates might be quite competitive with attack by oxygen atoms. For example, the best values for O atom attack on CH_4 give an activation energy of $10.5 \text{ kcal-mole}^{-1}$. However, the rate constants for reaction of O atoms with CH_3^\cdot may be comparable to CH_3^\cdot reaction with excited O_2 , since each reaction involves encounter between species having free valences. The actual concentration of excited O_2 made by an electrical discharge (concentration in the downstream effluent) may be as high as 10% of the total pressure.⁷ This would mean that in the experiments with CH_4 and HCl it would be reasonable to expect that concentrations of the order of 20 microns Hg (about 6×10^{14} molecules/cu cm) of $^1\Delta_g \text{O}_2$ were available in the reaction zone. Assuming that the reaction rates of $\text{O}_2(^1\Delta_g)$ and $\text{O}(^3P)$ atoms with CH_3 are similar, one would expect about a three-fold increase in oxidation rate in the electrical discharge experiment.

IV. Conclusions

Although both HCl (and Cl_2) catalyze the reaction of CH_4 with O and O_2 , the extent of the reaction at room temperature is small. We could detect no quantitative evidence for the formation of any carbonyls or carbonyl fragments during the course of the oxidations (this, however, does not preclude their presence as very short-lived intermediates in such systems). The presence or absence of ground-state O_2 produced no effect on the reaction of O atoms with CH_4 . Addition of O_2 to the N + NO stream gave no evidence of any rate changes. Discharged O_2 , however, significantly enhances the formation of combustion products. This result has been tentatively attributed to the presence of excited ($^1\Delta_g$) O_2 in the system. The reaction of CH_4 with OH radicals has been studied at room temperature, yielding a rate constant of $2.42 \times 10^{-15} \text{ cc/particle-sec}$.

V. Acknowledgements

The authors of this paper are deeply indebted to the American Gas Association for their support in this work.

Table I. ACTIVATION ENERGIES

<u>Reaction Number</u>	<u>Heat of Activation, kcal/g-mole</u>
(2)	4
(7)	11
(8)	8-9
(9)	8
(10)	≈ 53
(11)	≈ 58
(12)	≈ 60

Table II. RATE CONSTANTS FOR REACTIONS AT 300° K,
cu cm/particle-sec

$k_1 = \text{Unknown}$

$k_2 = 2.06 \times 10^{-11}$

$k_3 = 1.53 \times 10^{-14}$

k_4 , assumed to be between 10^{-10} - 10^{-11}

k_5 , assumed to be between 10^{-10} - 10^{-11}

$k_6 \sim 2 \times 10^{-13}$

Table III. ACTIVATION ENERGIES AND RATE CONSTANTS FOR HYDROCARBON-OXYGEN AND METHANE-OXYGEN REACTIONS (cc-mole⁻¹-sec⁻¹)

Species	<u>O₂(³Σ_g⁻)</u> (Ground State)	<u>O₂(¹Δ_g)</u> (Excited State)	<u>O₂(¹Σ_g⁺)</u> (Excited State)
		<u>With H₂</u>	
E _a	58 kcal-mole ⁻¹	35 kcal-mole ⁻¹	20 kcal-mole ⁻¹
k (300°K)	4 X 10 ⁻³⁰	1 X 10 ⁻¹⁴	1 X 10 ⁻⁶
k (1000°K)	3	3 X 10 ⁴	1 X 10 ⁵
		<u>With CH₄</u>	
E _a	57	34	19
k (300°K)	6 X 10 ⁻³⁰	4 X 10 ⁻¹⁴	2 X 10 ⁻⁶
k (1000°K)	6	6 X 10 ⁴	5 X 10 ⁶

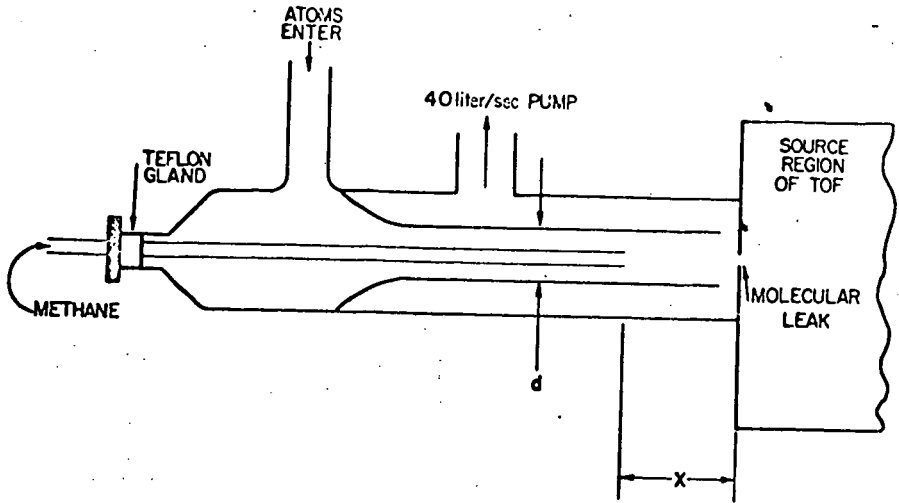


Figure 1 . FLOW REACTOR

A-1071396

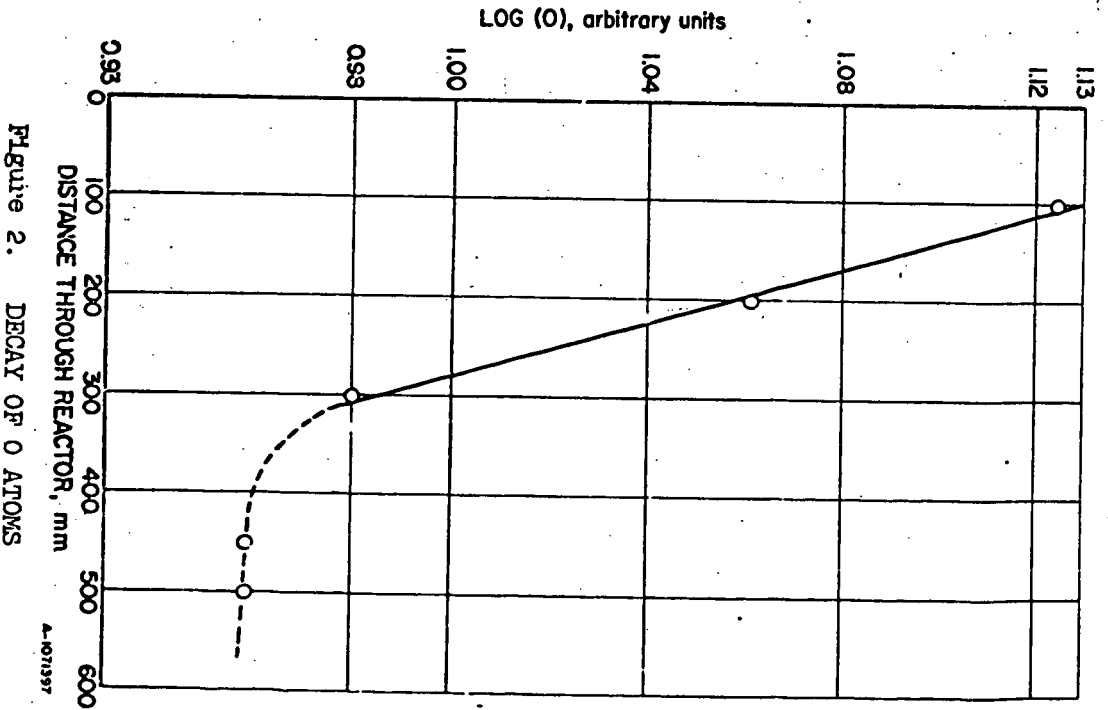
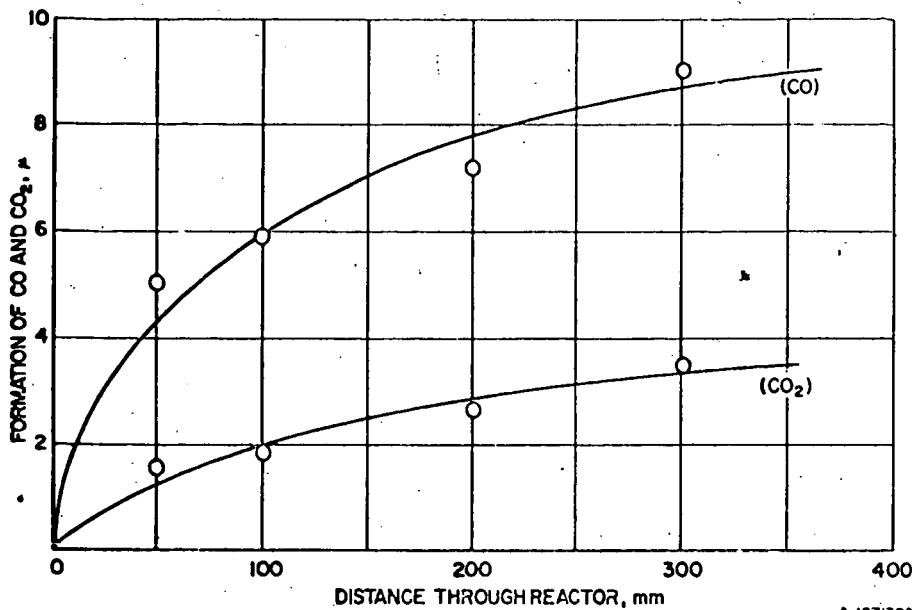


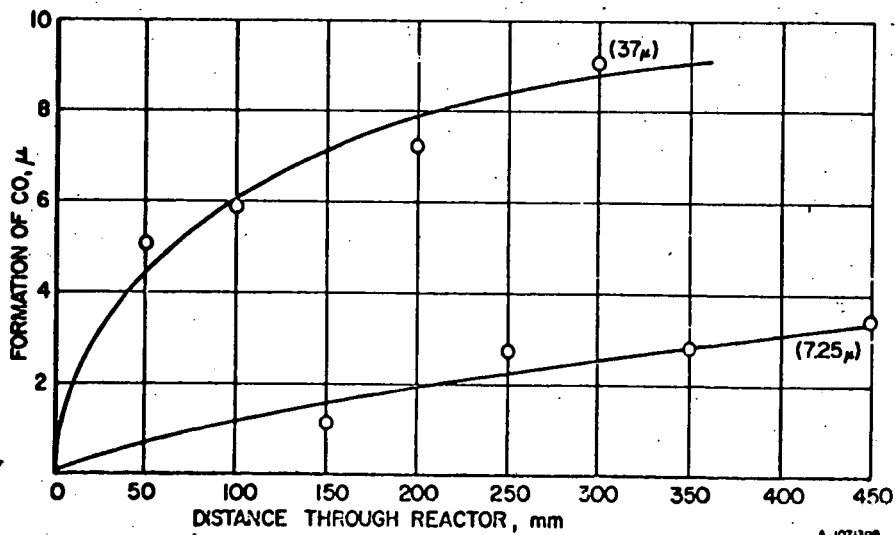
Figure 2. DECAY OF O ATOMS

A-1071397



A-1071398

Figure 3. RELATIVE FORMATION OF CO AND CO₂
WHEN 37 μ OF HCl IS ADDED



A-1071399

Figure 4. RELATIVE FORMATION OF CO FOR
DIFFERENT ADDITIONS OF HCl

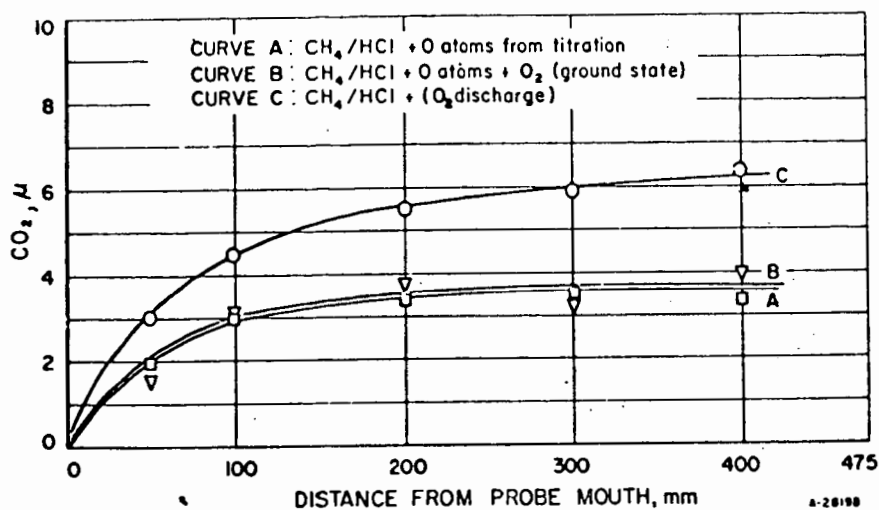


Figure 5. FORMATION OF CO_2 FOR VARIOUS $\text{CH}_4/\text{HCl}/\text{O}$ SYSTEMS

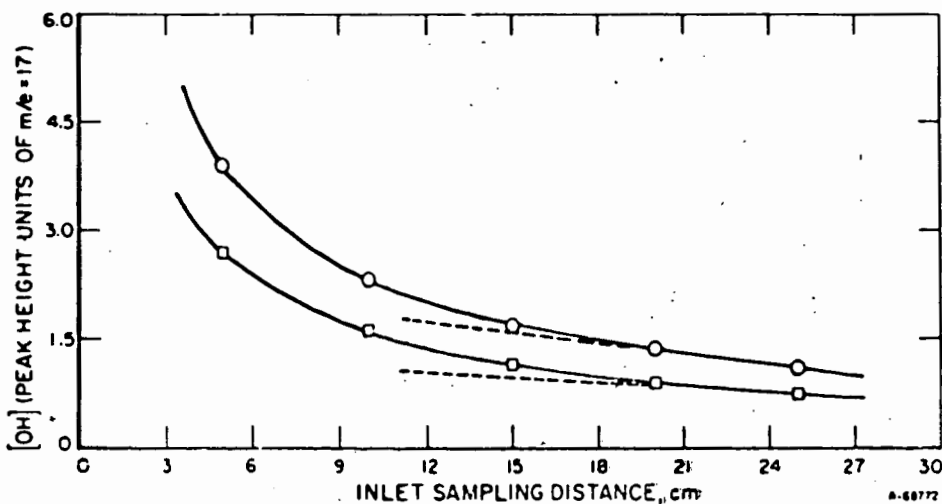


Figure 5. REACTION OF CH_4 WITH OH (at Different Initial Concentrations of OH)

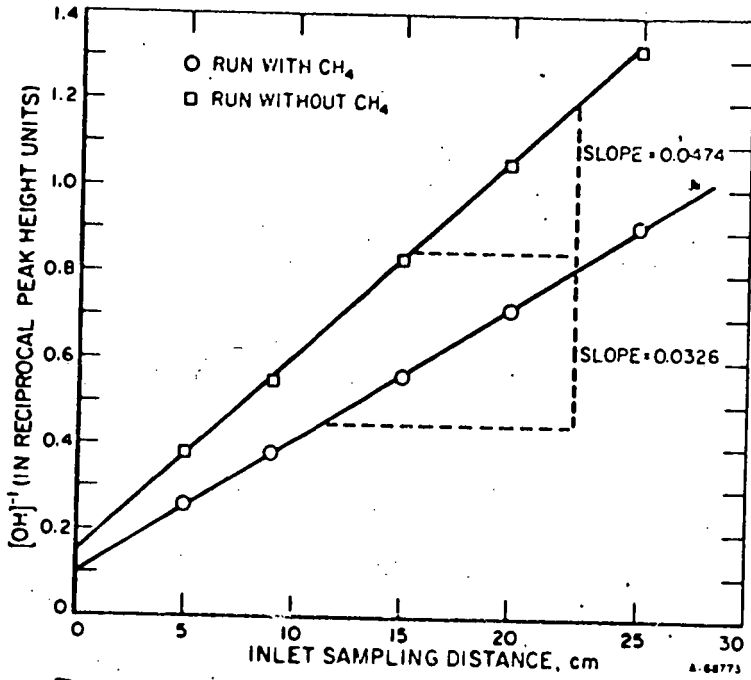


Figure 7. RECIPROCAL CONCENTRATION OF OH AS A FUNCTION OF DISTANCE FROM THE INLET DURING CH₄-OH REACTION